EJBCS

Eurasian Journal of Biological and Chemical Sciences (Eurasian J. Bio. Chem. Sci.)

Cilt:2 Volume: 1 Year: 2019

e-ISSN 2651-5237

EJBCS

Eurasian Journal of Biological and Chemical Sciences

Cilt: 2 Volume: 1 Year: 2019

Published Biannually

Corresponding Address
Gaziantep University, Faculty of Arts and Sciences, Department of Biology, Gaziantep, Turkey
E-mail: eurasianbiochemjournal@gmail.com / mtdogan1@gmail.com
Web: http://dergipark.org.tr/ejbcs

Owner / Publisher
Dr. Muhammet DOĞAN
This journal is peer-reviewed and published twice (June, December) a year.

e-ISSN 2651-5237

Eurasian J. Bio. Chem. Sci. 2(1): 1-6, 2019

EJBCS

Eurasian Journal of Biological and Chemical Sciences

Journal homepage: www.dergipark.gov.tr/ejbcs

Fabrication and Characterization of Polyvinyl Alcohol/Gelatin/ Silver Nanoparticle Nanocomposite Materials

Ayşen Aktürk[1,*], Büşra Cenik[1], Zeliha Aydoğdu[1], Melek Erol Taygun[1], Funda Karbancıoğlu Güler[2], Sadriye Küçükbayrak[1]

[1]*Istanbul Technical University, Faculty of Chemical and Metallurgical Engineering, Department of Chemical Engineering, Istanbul, Turkey*

[2] *Istanbul Technical University, Faculty of Chemical and Metallurgical Engineering, Department of Food Engineering, Istanbul, Turkey*

*Corresponding author : akturkay@itu.edu.tr
Orcid No: 0000-0003-2880-2999

Received : 30/09/2018
Accepted : 04/01/2019

Abstract: In this study, nanofibers containing silver nanoparticles were fabricated by electrospinnining. The blends of polyvinyl alcohol as a synthetic polymer and gelatin as a biopolymer were used to fabricate wound dressing material having antibacterial activity. Scanning electron microscope (SEM) analysis indicated that porous and interconnected nanofibrous structures were obtained for all blend compositions. X-Ray diffraction (XRD) results showed the existence of silver nanoparticles in the structures. The chemical changes related to crosslinking and the change of the structure in simulated body fluid were evaluated using Fourier transform infrared spectroscopy (FTIR). Antibacterial tests were performed to prove the antibacterial activity. The inductively coupled plasma optical emission spectrometry(ICP) results showed that controlled silver ion release was achieved. It was concluded that obtained nanofiber mats could be suitable candidates for wound dressing applications

Keywords: Silver Nanoparticles, Polyvinyl alcohol, Gelatin, Electrospinning, Wound Dressing

1. Introduction

Tissue engineering has evolved as a combination of engineering and life sciences principles to enhance tissue functions decades prior. The main direction of tissue engineering is to develop a suitable scaffold to mimic the extra cellular matrix (Shalumon et al., 2011). Tissue engineering provides a variety of techniques for scaffold production of which electrospinning is specifically noteworthy (Merkle et al., 2015). As of presently so numerous natural and synthetic polymers as well as their mixtures have been attempted in this case. A wide assortment of polymers are utilized in creating scaffolds using poly (vinyl alcohol), poly(ethyl oxide), poly(lactic acid), poly(glycolic acid), poly(lactic-co-glycolic acid), poly(caprolactone), or natural ones such as collagen, gelatin, silk, chitin, chitosan, alginate, hyaluronic acid which are natural extracellular matrix (ECM) analogs, due to their non-toxicity, improved biocompatibility, cell attachment and proliferation ability. In addition, polymers containing nanoparticles, and even metals and ceramics are used to increase cell migration and proliferation (Linh et al., 2010; Shalumon et al., 2011; Yang et al., 2011). Since the utilize of natural polymers have certain drawbacks like low stability, poisonous degradation products which can be destructive to the cells, the natural polymers are regularly mixed with synthetic polymers. Moreover this have upgraded mechanical properties, degradation stability and improved affinity to the cellular components (Shalumon et al., 2011). In any case, cytotoxic solvents such as 2,2,2-trifluoroethanol, 1,1,1,3,3,3-hexafluoro-2-propanol, trifluoroacetic acid, formic acid and dimethylformamide are generally utilized for their electrospinning (Yang et al., 2011).

Among the synthetic polymers mentioned above, PVA is one of a few situations which electrospun in aqueous solutions successfully to achieve nanofibrous mats with robust mechanical properties. As a semi-crystalline, biocompatible, non-toxic, hydrophilic polymer which has well chemical and thermal stability with incredible electrospinnability, it is one of the appropriate polymers that are readily mixed with natural polymers and crosslinked to form hydrogels (Fathollahipour et al., 2015; Yang et al., 2011). However, due to inadequate cell recognition sites, the bioactivity of PVA is significantly limited (Yang et al., 2011). Having natural plenitude, excellent biocompatibility and inalienable biodegradability in physiological situations, gelatin (GE) has been broadly utilized and contemplated with respect to numerous biomedical applications, such as surgical treatments, bone, skin and cartilage tissue engineering, wound or burn dressings (Rujitanaroj et al., 2008; Yang et al., 2011). By combining the advantages of PVA and GE, PVA /GE hybrid scaffolds are expected to

have robust mechanical properties and biocompatibility, while promising cell adhesion and biodegradability properties are achieved. Moreover, pure gelatin nanofibrous scaffolds are too delicate to ever be dealt with in practice. For this reason, hybridization of PVA with gelatin will significantly increase the flexibility of gelatinous scaffolds (Yang et al., 2011). The scaffold material in our study is a mixture of a PVA and a GE nanofiber obtained by one-step electrospinning as a wound dressing material.

Various investigations have been carried out with silver salts and silver compounds showing them as promising materials for wound management. With regard to the antimicrobial action, Ag salts and Ag compounds have been utilized as wound treatments in various physical shapes, such as beads, gels, films and fibers (Chun et al., 2010). For this reason, Ag NPs / polymer composites, which function as a bactericide, have been applied to complicated cases of infected burns, purulent wounds and wound healing matrix (Nguyen et al., 2010). In this study, microwave-assisted synthesis was performed to obtain soluble starch coated silver nanoparticles as colloidal solution and at that point this solution was blended with PVA/GE polymer solution to fabricate a novel wound dressing material displaying antibacterial activity.

2. Materials and Method

2.1 Materials

Polyvinyl alcohol (PVA, 95.5-96.5 % hydrolyzed, 85000-124000) was obtained from Acros. glutaraldehyde 50 wt. % in H_2O and gelatin from porcine skin were purchased from Sigma Aldrich. Acetic acid (glacial), tryptic soy broth (TSB), and tryptic soy agar (TSA) were supplied from Merck. Other than these materials, deionized water was used in order to prepare solutions.

2.2 Preparation of scaffolds containing silver nanoparticles

Soluble starch coated silver nanoparticles were synthesized by the method based on our previous study (Aktürk et al., 2019). This nanoparticle solution with mean particle size of 21 nm obtained by microwave-assisted green synthesis was mixed with acetic acid at 30/70 %v/v to prepare gelatin solution of 22 % wt/v. PVA solution was prepared at 10% wt/v using deionized water at 85 ℃ by stirring for 4 h. PVA solution was added to gelatin-silver nanoparticle solution (GE-Ag) at weight ratios of 3:1, 3:3, 3:5, and 3:7. The as prepared polymer solutions were electrospun at voltage of 25 kV, at spinning distance of 17 cm and at flow rate of 1 ml/h to fabricate nanocomposites with different Ag, PVA and GE compositions. Then these nanofiber mats were crosslinked under glutaraldehyde vapor by using glutaraldehyde solution (25ml) at 37 ℃ for 24h.

2.3 Silver ion release investigations

Nanofiber mats were soaked in simulated body fluid (SBF) for time intervals of 1, 7, 14, and 28 days. The concentrations of silver ions in SBF solution were measured.

2.4 Antibacterial activity

The antibacterial activity of the silver-containing nanofiber mats against *Escherichia coli* ATCC 25922, *Staphylococcus aureus* ATCC 29213 were investigated by disk diffusion method. Neat PVA/GE nanofiber mats were utilized as controls. Nanofiber mats were cut into disc with diameter of 30 mm and the crosslinking process was applied on them. Crosslinked nanofiber mats were sterilized under UV light for 2 hours (each for 1 hour). The bacteria were grown in TSB by incubation for 24 hours at 37 ° C. Then, bacterial concentrations of *E. coli* and *S. aureus* were set at 10^6 CFU / mL and at that point 100 µL of this bacterial suspension was spread to the TSA. Sterilized nanofiber mats were put on the inoculated TSA. After incubation at 37 °C for 24 hours, the antibacterial properties of the nanofiber mats were assessed by the formation of inhibition zones around the nanofiber mats diameter on each inoculated plate. All analyzes were performed in triplicate for each nanofiber mat.

2.4 Characterization of nanocomposite fiber mats

The surface morphology and microstructure of the nanocomposite fiber mats before and after immersion in SBF were observed by using scanning electron microscope (SEM). Before the observation, the surfaces of scaffolds were sputter coated (SC7620 sputter coater, Quorum Technologies Ltd, United Kingdom) with platinum for 120 s. For each experiment, the average fiber diameter and its standard deviation were analyzed by the help of an image visualization software (Image-J, National Institute of Health, USA) from about 50 measurements of the random fibers. X-ray Diffraction (XRD) (PANanalytical Xpert Pro) analysis was conducted to prove silver nanoparticles in nanofiber structure. The functional groups of the nanocomposite mats before and after crosslinking and before and after SBF immersion were investigated by Fourier-transform infrared (FT-IR) spectroscopy. FT-IR spectra were collected using Perkin Elmer Spectrum 100 model spectrometer in transmittance mode in the mid-IR region (4000-650 cm^{-1}). The concentrations of silver ions in the SBF solutions were measured by using inductively coupled plasma optical emission spectrometry (ICP-Perkin Elmer Optima 2100 DV model).

3. Results

Electrospinning was used to prepare highly porous nonwoven nanofibrous mats. Figure 1 shows SEM micrographs, average diameter and diameter distribution of the fiber mats made from PVA addition to GE-Ag blend at weight ratios of 3:1, 3:3, 3:5, and 3:7. As shown in Figure 1 defect free fibers are observed. When the PVA content increased, nanofiber mean diameter first decreased and then increased. Because the standard deviation of nanofiber size distributions are in a narrower range with the addition of PVA, it can be concluded that the nanofiber structures were formed more homogeneous by the aid of PVA.

The characteristics of Ag NPs in the nanofiber structures were investigated by using XRD measurements. The

representative XRD patterns of 3.1 PVA/GE-Ag and 3:7 PVA/GE-Ag nanocomposite mats are given in Figure 2. The 3:1 PVA/GE-Ag sample has diffraction peaks at 2Θ= 38.55˚, 44.804˚, 65.001˚, and 77.908˚, which belong to (111), (200), (220), and (311) crystal planes of Ag with cubic symmetry, individually. The 3:7 PVA/GE-Ag sample has these characteristic peaks at 38.783˚, 44.885˚, 64.998˚, and 77.944˚ (Celebioglu et al., 2014; Cheng et al., 2015; Islam and Yeum, 2013; Li et al., 2013; Mahanta and Valiyaveettil, 2012; Usman et al., 2016; Xiao et al., 2012; Zhang et al., 2016).

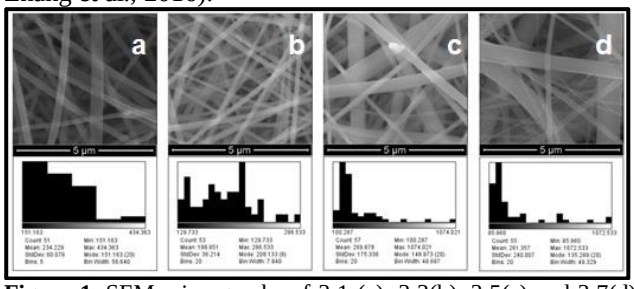

Figure 1. SEM micrographs of 3:1 (a), 3:3(b), 3:5(c) and 3:7(d) PVA/GE-Ag nanocomposites

For both nanofiber mats characteristic peaks of elemental Ag were observed, but, there were also additional peaks at about 28˚ corresponding to the indices (110) for Ag_3O_4 and 32˚ corresponding to the indices (120) for Ag_2O_2 which are the sign of oxidation of Ag (Celebioglu et al., 2014; Cheng et al., 2015). This is possibly originated from the further oxidation of Ag by PVA (Hong et al., 2006). With the addition of PVA into the structure, the intensity of the diffraction peak at around 19˚-21˚, which occurred due to the string inter and intra molecular hydrogen bonding corresponding with the crystalline peak of pure PVA, increased significantly (Cheng et al., 2015; Islam and Yeum, 2013; Lin et al., 2014; Park et al., 2011; Şimşek et al., 2016; Usman et al., 2016).

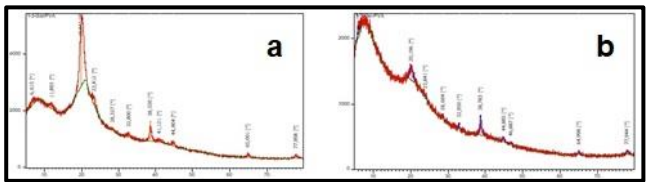

Figure 2. XRD spectra of 3:1 (a) and 3:7(b) PVA/GE-Ag nanocomposites

Because PVA and GE are water soluble, an e-spun GE and PVA nanofiber mat can partially or completely dissolve the when it comes in contact with an aqueous environment. When exposed to high ambient moisture, it may partially resolve and lose its fibrous structure (Rujitanaroj et al., 2008). Protection of nanofiber mat morphology and interfiber pores are critical for applications where the high surface area to volume ratio is advantageous (Destaye et al., 2013). More cross-linking is required to prolong the use of e-spun gelatin nanofibers in applications that need to be exposed to an aqueous medium or high humidity. Among the various chemical systems for cross-linking an e-spun gelatin (e.g., HDMI, EDC and GTA steam), GTA appears to be most economical and optimal material because it does not endanger the fibrous structure of the e-spun membrane (Rujitanaroj et al., 2008). The cross-linking reaction of PVA and GE was determined by using FTIR. The FTIR spectra of 3:1 PVA/GE-Ag and 3:7 PVA/GE-Ag nanocomposite mats were given in Figure 3.

The FTIR spectra of the nanofiber mats have the peaks of PVA which are characteristic broad spectrum at 3300 cm^{-1} (-OH stretching), 2916 cm^{-1} (symmetric -CH_2-), 1436 and 1087 cm^{-1} for C-O stretching and bending bonds, and 836 cm^{-1} for vibrational mode of C-C (Ghasemzadeh and Ghanaat, 2014; Kumar and Jaiswal, 2016; Martínez-Rodríguez et al., 2016). After the crosslinking reaction of PVA, the band at 1000-1140 cm^{-1} is observed due to the O-C-O vibration of the acetal group formation (Destaye et al., 2013). A new band at 1140 cm^{-1} is assigned to the symmetric C-C stretching mode in crystalline regions (Sui et al., 2012). This characteristic peak is well known to be sensitive marker for determining the degree of crystallinity of PVA. That is, the crystallization behavior of PVA is increased, which has an important role in preventing the dissolution of nanofibers in solutions (Sui et al., 2012). As seen in the spectra of 3:1 PVA/GE-Ag before and after crosslinking reaction, there is no differences for both structures except for the formation the band at 1143 cm^{-1} after crosslinking reaction. Due to the ratio of PVA is higher than GE at this nanofiber structure, the crosslinking reaction effect related to PVA crosslinking was seen more dominant.

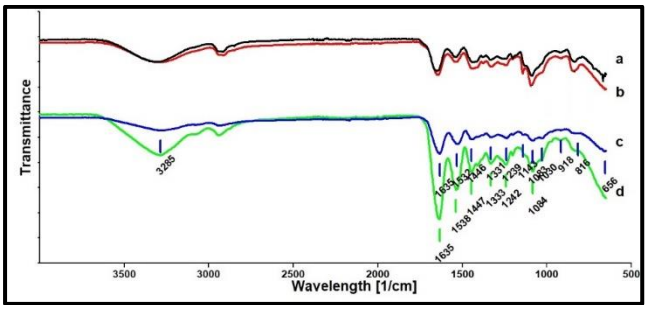

Figure 3. FTIR spectra of 3:1 PVA/GE-Ag before(a)/ after crosslinking (b) and 3:7 PVA/GE-Ag nanocomposites before(d)/after(c)crosslinking

The ordinary band assignments for gelatin detailed in the literature are amide A (N-H stretching vibration) found at around 3300 cm^{-1}; amide I (C=O stretch) found at 1640 cm^{-1}; amide II located between 1535 and 1554 cm^{-1} and amide III observed at 1240 cm^{-1}. The amide II and amide III groups result from the bending vibration of N-H groups and the stretching vibrations of C-N groups and interaction between these two modes (Gao et al., 2013). When the FTIR spectra of the 3:7 PVA/GE-Ag structure before and after crosslinking are examined, it is seen that the intensity of N-H group stretching vibration observed at 3285 cm^{-1} and the N-H group bending vibrations observed at 1635 cm^{-1} decrease relatively after cross-linking. The intensity of groups between 1250 and 1160 cm^{-1} decreased, which demonstrated the amount of C-N-C groups decreased (Lu et al., 2015). Additionally, the formation of the band at 1143 cm^{-1} was observed, which is the sign of the crosslinking reaction of PVA.

The success of crosslinking was checked by the immersion of nanofibrous mats in SBF. The SEM images of soaked nanofibers in SBF were given in Figure 4. As seen the images at day 0, the fibers fused together after cross-linking because of the existence of the water in moisture rich glutaraldehyde vapor (Gönen et al., 2016).

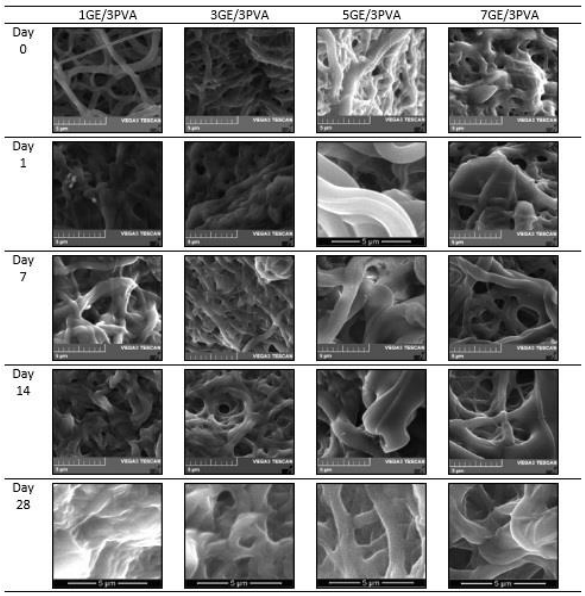

Figure 4. SEM micrographs of 3:1 (a), 3:3(b), 3:5(c) and 3:7(d) PVA/GE-Ag nanocomposites in SBF in different time intervals.

The change of chemical structures of 3:1 PVA/GE-Ag and 3:7 PVA/GE-Ag nanofiber mats were determined after SBF immersion for 28 days by using FTIR. As seen in the Figure 5, the 3:1 PVA/GE-Ag nanofiber mat was more effected than 3:7 PVA/GE-Ag nanofiber mat. It was observed that the peak at 1143 cm^{-1} showing the crystallinity of the 3:1 PVA/GE-Ag structure disappeared after the immersion in SBF.

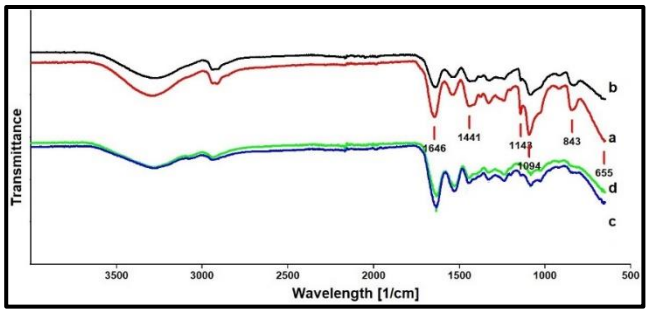

Figure 5. SEM micrographs of 3:1 (a), 3:3(b), 3:5(c) and 3:7(d) PVA/GE-Ag nanocomposites

The silver ion contents of the SBF solutions after the immersion of nanofiber composite mats were measured to determine the potential of the nanofiber mats for antibacterial and biomedical applications. During this method the ratio of nanofiber to SBF was taken as 0.25 mg/ml. Figure 6 illustrates the amount of silver ion releases into SBF as a function of time.

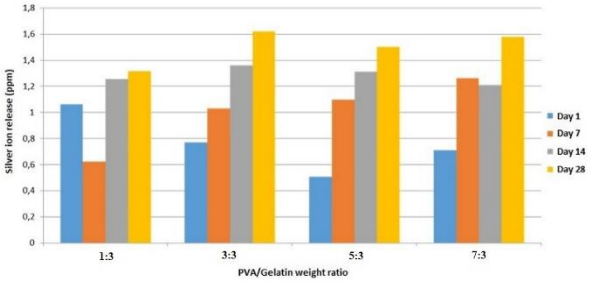

Figure 6. Silver ion release of nanocomposites in SBF in different time intervals.

Antibacterial tests were performed with 3: 7 PVA / GE-Ag sample since it has both stability in SBF and silver ion release below toxic level. The antibacterial properties of 3:7 PVA/GE-Ag nanofibers against gram-negative *E. coli* and gram-positive *S. aureus* were investigated by agar diffusion test measuring bacterial growth inhibition zone. Figure 7 shows images of the inhibition zones of the 3:7 PVA/GE-Ag nanofibers against *E. Coli* and *S. aureus* using 3:7 PVA/GE as the control.

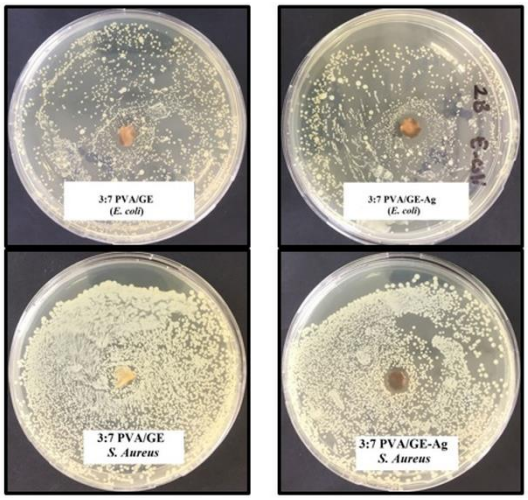

Figure 7. Antimicrobial activity of 3:7 PVA/GE-Ag nanofiber mats against *E. Coli* and *S. aureus*.

The inhibition zone of the surrounding Ag NP-containing fibers can be clearly observed. However, the PVA/GE nanofibers without AgNPs did not show any inhibition region. The results are dependent on the presence of antibacterial ability of AgNPs in the fibers. In particular, the 3:7 PVA/GE-Ag nanofibers were more effective against *E. coli* than *S. aureus.*

4. Discussion

A perfect wound dressing ought to be porous to preserve a wet environment and anticipate lack of hydration. Subsequently it ought to have high porousness, a high degree of swelling, and little weight loss (Li et al., 2013). To make the structure suitable for wound dressing applications silver nanoparticle containing GE/PVA nanofiber mats were cross-linked by saturated vapor from 50 vol% GTA aqueous solution for 24 h, followed by a heat treatment at 120 ℃ for 2h in this study. The formation of uniform fiber structures at nanofiber mats elucidate that the concentration and the viscosity of the electrospinning

solutions were at the optimal levels. The leaching behavior of PVA/GE-Ag nanofibers were evaluated using static method under equal conditions. Based on the SEM images, the more content of gelatin in the structure, there is smaller dissolution and more retention of the morphological structure of the crosslinked samples in SBF for 1, 7, 14 and 28 days. The Ag^+ ion concentration which is effective to inhibite the growth of bacteria was published at above 0.1 ppb and it was reported that below 2.3 ppm and 1.7 ppm have no effect on HaCat keratinocytes and human epidermal keratinocytes, respectively (Zhao et al., 2012). The maximum silver ion amount released from these nanofiber mats was 1.6224 ppm, which is under the toxic level. The accumulative Ag^+ release of all the nanofibers show similar trend. This recommends that the fibers ought to have sound antibacterial capacity and little cytotoxicity.

5. Conclusions

In this study, it was aimed to fabricate silver nanoparticle containing polyvinyl alcohol/gelatin nanofiber mats. The results showed that silver nanoparticles were incorporated in the structure successfully. The FTIR and SEM results showed that nanofiber structure of the blend at high gelatin ratio retained and there is no chemical changes after SBF immersion in SBF. The antibacterial tests performed with this nanofiber mat showed activity against *E. coli and S. aureus*. The obtained results demonstrates that this nanocomposite has the potential to use in wound dressing applications.

References

Aktürk A, Erol Taygun M, Karbancıoğlu Güler F, Goller Gultekin, and Küçükbayrak S 2019. Fabrication of antibacterial polyvinylalcohol nanocomposite mats with soluble starch coated silver nanoparticles. Colloids and Surfaces A 562: 255-262

Asran AS, Henning S, and Michler GH 2010. Polyvinyl alcohol–collagen–hydroxyapatite biocomposite nanofibrous scaffold: mimicking the key features of natural bone at the nanoscale level. Polymer, 51(4): 868-876.

Celebioglu A, Aytac Z, Umu OC, Dana A, Tekinay T, and Uyar T 2014. One-step synthesis of size-tunable Ag nanoparticles incorporated in electrospun PVA/cyclodextrin nanofibers. Carbohydrate polymers, 99: 808-816.

Cheng Z, Zhang F, Liu W, Cui L, and Kang L 2015. A novel preparation for a PVA/l-histidine/AgNPs membrane and its antibacterial property. RSC Advances, 5(67): 54182-54187.

Chun JY, Kang HK, Jeong L, Kang YO, Oh J-E, Yeo I-S, Jung SY, Park WH, and Min B-M 2010. Epidermal cellular response to poly (vinyl alcohol) nanofibers containing silver nanoparticles. Colloids and Surfaces B: Biointerfaces, 78(2): 334-342.

Destaye AG, Lin CK, and Lee CK 2013. Glutaraldehyde vapor cross-linked nanofibrous PVA mat with in situ formed silver nanoparticles. ACS applied materials & interfaces, 5(11): 4745-4752.

Fathollahipour S, Abouei Mehrizi A, Ghaee A, and Koosha M 2015. Electrospinning of PVA/chitosan nanocomposite nanofibers containing gelatin nanoparticles as a dual drug delivery system. Journal of Biomedical Materials Research Part A, 103(12): 3852-3862.

Gao C, Gao Q, Li Y, Rahaman MN, Teramoto A, and Abe K 2013. In vitro evaluation of electrospun gelatin- bioactive glass hybrid scaffolds for bone regeneration. Journal of Applied Polymer Science, 127(4): 2588-2599.

Ghasemzadeh H, and Ghanaat F 2014. Antimicrobial alginate/PVA silver nanocomposite hydrogel, synthesis and characterization. Journal of Polymer Research, 21(3): 355.

Gönen SÖ, Taygun ME, and Küçükbayrak S 2016. Fabrication of bioactive glass containing nanocomposite fiber mats for bone tissue engineering applications. Composite Structures, 13: 96-106.

Hong KH, Park JL, Sul IH, Youk JH, and Kang TJ 2006. Preparation of antimicrobial poly (vinyl alcohol) nanofibers containing silver nanoparticles. Journal of Polymer Science Part B: Polymer Physics, 44(17): 2468-2474.

Islam MS, and Yeum JH 2013. Electrospun pullulan/poly (vinyl alcohol)/silver hybrid nanofibers: preparation and property characterization for antibacterial activity. Colloids and Surfaces A: Physicochemical and Engineering Aspects, 436: 279-286.

Kumar A, and Jaiswal M 2016. Design and in vitro investigation of nanocomposite hydrogel based in situ spray dressing for chronic wounds and synthesis of silver nanoparticles using green chemistry. Journal of Applied Polymer Science, 133(14):43260.

Li C, Fu R, Yu C, Li Z, Guan H, Hu D, Zhao D, and Lu L 2013. Silver nanoparticle/chitosan oligosaccharide/poly (vinyl alcohol) nanofibers as wound dressings: a preclinical study. International journal of nanomedicine, 8:4131.

Lin S, Wang RZ, Yi Y, Wang Z, Hao LM, Wu JH, Hu GH, and He H 2014. Facile and green fabrication of electrospun poly (vinyl alcohol) nanofibrous mats doped with narrowly dispersed silver nanoparticles. International journal of nanomedicine, 9:3937.

Linh NTB, Min YK, Song HY, and Lee BT 2010. Fabrication of polyvinyl alcohol/gelatin nanofiber composites and evaluation of their material properties. Journal of Biomedical Materials Research Part B: Applied Biomaterials, 95(1): 184-191.

Lu W, Ma M, Xu H, Zhang B, Cao X, and Guo Y 2015. Gelatin nanofibers prepared by spiral-electrospinning and cross-linked by vapor and liquid-phase glutaraldehyde. Materials Letters, 140(1-4.

Mahanta N, and Valiyaveettil S 2012. In situ preparation of silver nanoparticles on biocompatible methacrylated poly (vinyl alcohol) and cellulose based polymeric nanofibers. RSC Advances, 2(30): 11389-11396.

Martínez-Rodríguez M, Garza-Navarro M, Moreno-Cortez I, Lucio-Porto R, and González-González V 2016. Silver/polysaccharide-based nanofibrous materials synthesized from green chemistry approach. Carbohydrate polymers, 136: 46-53.

Merkle VM, Tran PL, Hutchinson M, Ammann KR, DeCook K, Wu X, and Slepian MJ 2015. Core–shell PVA/gelatin electrospun nanofibers promote human umbilical vein endothelial cell and smooth muscle cell proliferation and migration. Acta biomaterialia, 27: 77-87.

Nguyen TH, Lee KH, and Lee BT 2010. Fabrication of Ag nanoparticles dispersed in PVA nanowire mats by microwave irradiation and electro-spinning. Materials Science and Engineering: C, 30(7): 944-950.

Park JH, Kim IK, Choi JY, Karim MR, Cheong IW, Oh W, and Yeum JH 2011. Electrospinning fabrication of poly (vinyl alcohol)/waterborne polyurethane/silver composite nanofibre mats in aqueous solution for anti-bacterial exploits. Polymers & Polymer Composites, 19(9): 753.

Rujitanaroj P, Pimpha N, and Supaphol P 2008. Wound-dressing materials with antibacterial activity from electrospun gelatin fiber mats containing silver nanoparticles. Polymer, 49(21): 4723-4732.

Shalumon K, Anulekha K, Chennazhi KP, Tamura H, Nair S, and Jayakumar R 2011. Fabrication of chitosan/poly (caprolactone) nanofibrous scaffold for bone and skin tissue engineering. International journal of biological macromolecules, 48(4): 571-576.

Son WK, Youk JH, and Park WH 2006. Antimicrobial cellulose acetate nanofibers containing silver nanoparticles. Carbohydrate Polymers, 65(4): 430-434.

Sui C, Li C, Guo X, Cheng T, Gao Y, Zhou G, Gong J, and Du J 2012. Facile synthesis of silver nanoparticles-modified PVA/$H_4SiW_{12}O_{40}$ nanofibers-based electrospinning to enhance photocatalytic activity. Applied Surface Science, 258(18): 7105-7111.

Şimşek M, Rzayev ZM, and Bunyatova U 2016. Multifunctional electroactive electrospun nanofiber structures from water solution blends of PVA/ODA–MMT and poly (maleic acid-alt-acrylic acid): Effects of Ag, organoclay, structural rearrangement and NaOH doping factors. Advances in Natural Sciences: Nanoscience and Nanotechnology, 7(2): 025009

Tsai RY, Hung SC, Lai JY, Wang DM, and Hsieh HJ 2014. Electrospun chitosan–gelatin–polyvinyl alcohol hybrid nanofibrous mats: Production and characterization. Journal of the Taiwan Institute of Chemical Engineers, 45(4): 1975-1981

Usman A, Hussain Z, Riaz A, and Khan AN 2016. Enhanced mechanical, thermal and antimicrobial properties of poly (vinyl alcohol)/graphene oxide/starch/silver nanocomposites films. Carbohydrate polymers, 153: 592-599.

Xiao S, Xu W, Ma H, and Fang X 2012. Size-tunable Ag nanoparticles immobilized in electrospun nanofibers: synthesis, characterization, and application for catalytic reduction of 4-nitrophenol. RSC Advances, 2(1): 319-327.

Yang C, Wu X, Zhao Y, Xu L, and Wei S 2011. Nanofibrous scaffold prepared by electrospinning of poly (vinyl alcohol)/gelatin aqueous solutions. Journal of Applied Polymer Science, 121(5): 3047-3055.

Yang D, Li Y, and Nie J 2007. Preparation of gelatin/PVA nanofibers and their potential application in controlled release of drugs. Carbohydrate Polymers, 69(3): 538-543.

Zhang Z, Wu Y, Wang Z, Zou X, Zhao Y, and Sun L 2016. Fabrication of silver nanoparticles embedded into polyvinyl alcohol (Ag/PVA) composite nanofibrous films through electrospinning for antibacterial and surface-enhanced Raman scattering (SERS) activities. Materials Science and Engineering: C, 69: 462-469.

Zhao Y, Zhou Y, Wu X, Wang L, Xu L, and Wei S 2012. A facile method for electrospinning of Ag nanoparticles/poly (vinyl alcohol)/carboxymethyl-chitosan nanofibers. Applied Surface Science, 258(22): 8867-8873.

Eurasian J. Bio. Chem. Sci. 2(1): 7-10, 2019

EJBCS

Eurasian Journal of Biological and Chemical Sciences

Journal homepage: www.dergipark.gov.tr/ejbcs

The first record for *Plutella xylostella* (Linnaeus, 1758) (Lepidoptera: Plutellidae) in Çanakkale province of Turkey and external and genital morphology of the species

Erol Atay[1*], Levent Efil[2], Mahmut Tatlı[3], Berrin Alaca[4]

[1*]*Department of Biology, Faculty of Arts and Sciences, Mustafa Kemal University, Hatay, Turkey*
[2]*Faculty of Agriculture, Dep. of Plant Protection, Çanakkale 18 March University, Çanakkale, Turkey*
[3]*Institute of Science, Mustafa Kemal University, Hatay, Turkey*
[4]*Ministry of Agriculture and Forestry, Çanakkale Provincial Directorate, Turkey*

*Corresponding author :eatay@mku.edu.tr
Orcid No: 0000-0002-5274-1025

Received : 07/12/2018
Accepted : 10/05/2019

Abstract: This study was conducted in the field and the laboratory. *Plutella xylostella* was captured in cabbage fields in central district of Canakkale, Ezine district and Ayvacık district during the day and night field studies. For during the day atrap, and for at night light traps were used. In the field studies, totally 35 male and 108 female specimens were collected. Specimens were dissected and male genitalia and wings microscope slides were prepared in the laboratory. We described the external and genital morphology of the male *Plutella xylostella* and diagnostic morphological features in detail. As a result of the study, *Plutella xylostella* is a new record for Çanakkale province.
Keywords: Çanakkale, Lepidoptera, *Plutella xylostella*, Plutellidae.

Türkiye Çanakkale İlinde Plutella xylostella (Linnaeus, 1758) (Lepidoptera: Plutellidae)'nın İlk Kaydı ve Türün Dış ve Genital Morfolojisi

Özet: Bu çalışma saha ve laboratuvar çalışmaları şeklinde gerçekleştirilmiştir. *Plutella xylostella*, Çanakkale ili Merkez ilçesi, Ezine ilçesi, Ayvacık ilçesi ile Ezine ilçesindeki lahana tarlalarında gündüz ve gece sürdürülen arazi çalışmalarında yakalandı. Gündüzleri atrap, geceleri ise ışık tuzakları kullanılmıştır. Saha çalışmalarında toplam 35 erkek ve 108 dişi toplanmıştır. Örnekler laboratuvarda preparat yapımı için hazırlandı, erkek genital ve kanat preparatları yapıldı. *Plutella xylostella*'nın dış morfolojisi ve erkek genital organları ayrıntılı olarak tanımlandı. Çalışma sonucu olarak *Plutella xylostella* Çanakkale için ilk kayıttır.
Anahtar Kelimeler: Çanakkale, Lepidoptera, *Plutella xylostella*, Plutellidae.

1. Introduction

The family Plutellidae *sensu stricto* comprised 5 genera containing 58 species. *Eidophasia* (11 species), *Lunakia* (1 species), *Plutella* (22 species, 12 attributable to *Plutella sensu stricto*), *Leuroperna* (2 species) and *Rhigognostis* (22 species). Two further genera, the brachypterous subantarctic *Embryonopsis* (1 species) and the Australasian *Proditrix* (2 species) are only tentatively associated with the family (Robinson and Sattler, 2001). Diamondback moths, family Plutellidae, include four subfamilies Ypsolophinae, Plutellinae, Scythropiinae and Praydinae (Heppner, 2008). *Plutella* Schrank, 1802, is poorly defined genus with a worldwide distribution containing 22 species. The type species, *Plutella xylostella* (L.), Diamondback moth or Cabbage moth, is a notorious migratory pest of brassicaccous crops (Robinson and Sattler, 2001).

The diamondblack moth, *Plutella xylostella* (L.) (Lepidoptera: Plutellidae), is one of the most serious pests of cultivated Brassicaceae worldwide (Moriuti, 1986; Avcı and Özbek, 1995; Hagerty et al., 2008; Bertolaccini et al., 2011; Pengyan et al., 2012; De Bortoli et al., 2014; Bacci et al., 2018). This crucifer specialist may have its origin in Europe, South Africa, or East Asia, but is now present worldwide wherever its host plants exist (De Bortoli et al., 2014). The authors (De Bortoli et al., 2014) gave the following information about the larval feding of the species; in the first instar, the larvae enter into the leaf parenchyma and feed between the upper and lower surfaces of leaves creating mines. In the second instar, the larvae leave the mines, and from the second to the third instar, they feed on the leaves, destroying the leaf tissue except for the upper epidermis, leaving transparent "windows" in the leaves. Fourth-instar larvae feed on both side of the leaves. This insect has a short life cycle, around 18 days, and its population may increase up to 60 fold from one generation to the next.

Avcı and Özbek (1995) state that this insect is damaging in cabbage and other Crucifer species in more than one hundred countries. Among the reasons for their significant detriment are the factors such as the ability to adapt to

different climatic conditions, the high reproductive power, and the resistance to all the pesticides used. The authors also report that the insect has the ability to migrate to far distances, migrating to distances over 1000 km or more by air flow through atmospheric pressure. Although this species has the ability to migrate to long distances, the ability of its natural enemies to migrate is very limited. This situation causes the insect to adapt more easily and cause significant damage in the new Crucifer cultivated fields. In Canada, *P. xylostella* leaves around 164 eggs per cabbage plant and gives 4-5 progeny per year. In Israel, the female of this species leaves an average of 280 eggs and gives 10 progeny per year. (Avcı and Özbek 1995).

Avcı and Özbek (1995), in their study of cabbage fields in Erzurum province in 1995, reported that *P. xylostella* significantly damaged to the plant, larvae fed on the lower face of the leaf and riddled like griddle. Adult female butterflies usually lay their eggs on the lower surface of the leaf of the host plant as individually or in groups of 2-8. In field conditions, the eggs are opened in 2-7 (4) days, the larval period is 8-18 (12) and the duration of pupa is 3-8 (5) days, thus the insect development is completed in 13-31 (21) days. (Avcı and Özbek 1995).

There are two species (*P. porrectella* (L., 1758); *P. xylostella*) belonging to the genus *Plutella* in Turkey (Koçak and Kemal, 2009; 2018). The first attempt on the checklist of the Turkish moths was listed by Koçak and Kemal (2006, 2007; 2018). Totally 4604 moth species were listed together with their synonymous named and updated provincial distributions. Later, the authors (Koçak and Kemal, 2009) reported that the Turkey Lepidoptera fauna was 5128 species belonging to 76 families. In addition, a total of 343 lepidoptera species, 240 Heterocera and 103 Rhopalocera, belonging to the province of Çanakkale were listed by the same authors. The species belonging to the genus *Plutella* are not found in Çanakkale. *P. xylostella* is a new record for the the lepidoptera fauna of Çanakkale.

2. Materials and Method

The study was conducted in the field and the laboratory.

2.1. Field Studies

Field studies were carried out in cabbage fields in Çanakkale province in September and October 2018. All the field works were done under suitable weather conditions (without precipitation and strong winds), and works started early in the morning and continued until sunset. *Plutella xylostella* was caught in various cabbage fields with light trap at night and atrap (butterfly net) during day. In the field studies, totally 35 male and 108 female specimens were collected.

2.1. Laboratory Studies

Before they were losing body water, the collected specimens were sorted according to body sizes, and were needed with a number 0 insect needles that matched the size of the custom sized boards, strain and inhibition couples were strained in laboratory work. For the drying of the stretched specimens, they kept at room temperature for two weeks in a dark and dry place. Male genital organ was prepared for the identification of the species following morphological examinations and measurements on the male specimens. The needling of the moths, stretching of the wings and genital organ preparations were done accordingly the methods which defined in Atay's work (2006). The major taxonomic characters described. Important morphological organs of *Plutella xylostella* were photographed. The specimens stored at the Biology Department of Mustafa Kemal University in Hatay.

3. Results

Genus *Plutella* Schrank, 1802 **(Plutellidae)**

Syn: *Anadetia* Hübner, [1825]; *Euota* Hübner, [1825]; *Creagria* Sodoffsky, 1837; *Evota* Agassiz, 1847; *Pseudoplutella* Baraniak, 2007 (Koçak and Kemal, 2009; 2018).

***Plutella xylostella* (Linnaeus, 1758)**

Plutella Tinea xylostella Linnaeus, 1758, Sys. Nat. Ed.: 538.
Cerostoma maculipennis Curtis, 1832, Brit. Entomol. Pl. 420.
Plutella cruciferarum Zeller, 1843, Stett. Entomol. Ztg., 4:1281.
Plutella brassicella Fitch, 1856, Rep. Nox. Inst. New York, 1:170.
Plutella limbipennella Clemens, 1860, Proc. Acad. Nat. Sci. Philad., 12:6.
Plutella mollipedella Clemens, 1860, Proc. Acad. Nat. Sci. Philad., 12:6.
Gelechia cicarella Rondani, 1876, Bull.Soc. Entomol. Ital., 8:20.
Tinea galeatella Mabille, 1888, Miss. Sci. Cap. Horn, 6:34.
Cerostom dubiosella Beutenmuller, 1839, Can. Entomol., 21:27. (Moriuti, 1986)

The distribution of *Plutella xylostella* in Turkey; Adana, Ankara, Bitlis, Diyarbakır, Gaziantep, Hakkari, Hatay, Mersin, İstanbul, Kayseri, Konya, Malatya, Muğla, Muş, Şanlıurfa, Van, Kırıkkale (Koçak and Kemal, 2009; 2018).

The distribution of *Plutella xylostella* in the world; Belgium, Austria, Albania, Afghanistan, Germany, Azerbaijan, United Arab Emirates, Switzerland, Czech Republic, Algeria, Denmark, Spain, France, Finland, Great Britain, Greece, Bulgaria, Hungary, Israel, India, Italy, Iceland, Ireland, Iran, Iraq, Lebanon, Luxembourg, Latvia, Lithuania, Malta, Moldova, Malaysia, Netherlands, Norway, Portugal, Poland, Romania, Saudi Arabia, Sweden, Thailand, Tunisia, Slovakia, Turkmenistan, Ukraine, Yugoslavia, Russia, Yemen, South Africa (Karsholt and Razowski, 1996; Koçak and Kemal, 2018).

Material Examined: Çanakkale-Center-Kumkale Village (39°59'01" N; 26°13'22" E, 42 m.); Çanakkale-Center-Tevfikiye Village (39°57'12" N; 26°14'43" E, 75 m.); Çanakkale- Center-Halileli Village (39°58'16" N; 26°16'34" E, 58 m.); Çanakkale-Ayvacık-Kösedere Village (39°39'43" N; 26°90'54" E, 5 m.); Çanakkale-Ezine-Hisaralan Village (39°76'18" N; 26°28'69" E, 185 m.); Çanakkale-Ezine-Kemallı Village (39°75'93" N; 26°23'54"

E, 160 m.); Çanakkale-Bayramiç (39°48'48" N; 26°35'42" E, 118 m.)
01.IX.2018 6♂, 20♀; 15.IX.2018 6♂, 21♀; 29.IX.2018 8♂, 20♀; 13.X.2018 6♂, 35♀; 27.X.2018 9♂, 12♀.

Measurements of the Adults

Body Length ♂: 5 mm, ♀: 5-6 mm.
Wingspan ♂: 13 mm, ♀: 13-14 mm.

Male (Figure 1): The adults of *Plutella xylostella* 5-6 mm in size and greyish brown in colour. There are four diamond shaped whitish beige patterns along the costal edge of the forewings, giving the moth its common name. These diamond shapes are more distinct in males than those of females.

On the head vertex and frons yellowish brown, scales dirty white tipped, these scales are long and pretty fluffy (Figure 2). Antenna fuscous light brownish with black rings and with short setae; about ¾ length of forewing. Labial palpus well developed, long, curled up, well visible; its second segment with forward directed triangular tuft. Haustellum is well developed and naked. Eyes are round, large and dark brown. On the head ocelli well developed. (Figure 3). Veins of forewing and hindwing of *Plutella xylostella* are in Figure 3.

Forewings are long, too narrow and pointed, its length 3,6 times longer than its width. The ground colour of the forewing is grayish brown with small yellowish brown stains. There are four diamond shaped whitish beige patterns along the costal edge of the forewings. Hindwings are narrow and its length 3,7 times longer than its width. The ground colour of the hindwings brown.

The male genital organ is in Figure 4.

Valva is long and very broad, sclerotized and large round at the end, its length 2 times longer than its width and covered with long and frequent hairs. Tegumen is strongly sclerotized. Aedeagus is long and straight, sharply pointed, needle like with bulbus base and pair of lateral hooks, without cornuti. Saccus is long and broad, triangular.

The larvae and damage shape of *P. xylostella* are in Figure 5.

Figure 1. Adults of *Plutella xylostella.*

Figure 2. The head structure of *Plutella xylostella.*

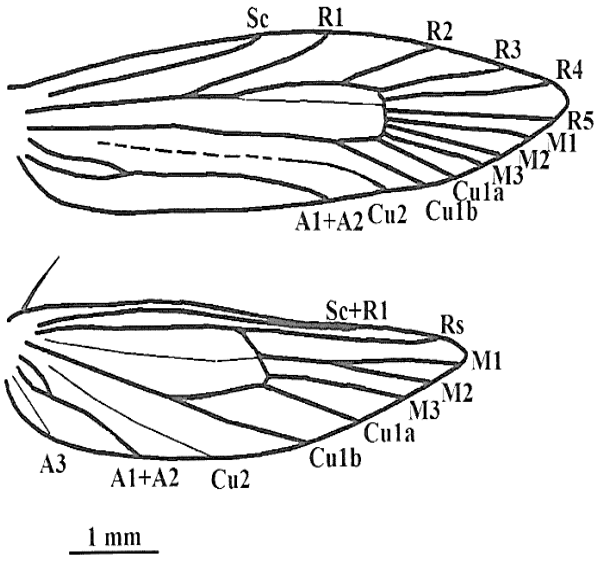

Figure 3. Veins of forewing and hindwing of *Plutella xylostella*

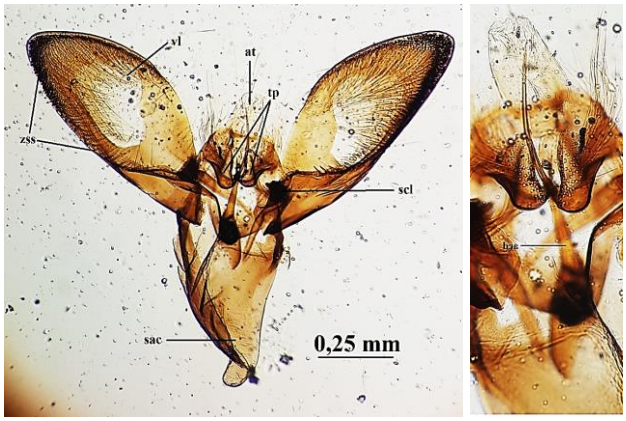

Figure 4. The Male Genitalia of *Plutella xylostella* and Aedeagus (aed = aedeagus, at = anal tube, sac = saccus, scl = sacculus, tp = teguminal process, vl = valva, zss = zone of spiniform setae.

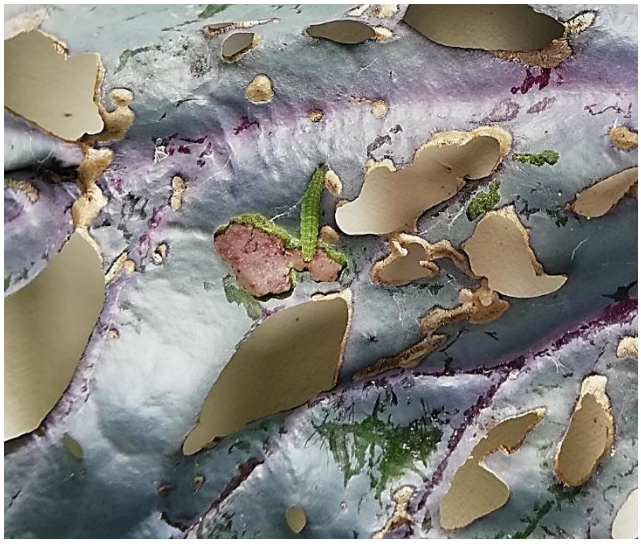

Figure 5. The larvae and damage shape of *P. xylostella*

4. Discussion

In this study, we described the external and genital morphology of the male *Plutella xylostella*. The important taxonomic characters belong to *P. xylostella* were described in detail. Each one of the external and genital taxonomic characters was measured with digital caliper and stereo microscope. This species is a new record for the the lepidoptera fauna of Çanakkale.

References

Atay E 2006. The identity of *Parapoynx affinialis* (Guenée, 1854) (Lepidoptera, Crambidae, Nymphulinae) in Turkey. J of Entom 3: 76-81.

Avcı Ü, Özbek H 1995. Erzurum'da yaprak güvesi *Plutella xylostella* (L.) (Lep: Yponomeutidae)'nın biyolojisi, zararı ve mücadelesi üzerine bazı gözlemler. Atatürk Üni Zir Fak Der 26: 363-374.

Bacci L, Rosado JF, Picanço MC, Gonring AHR, Galdino TVS Martins JC 2018. Failure control of *Plutella xylostella* (Lepidoptera: Plutellidae) and selectivity of their natural enemies to different insecticides. J of Plant Protec Res 58: 161-167.

Bertolaccini I, Sanchez DE, Arregui MC, Favaro JC Theiler N 2011. Mortality of *Plutella xylostella* (Lepidoptera, Plutellidae) by parasitoids in the province of Santa Fe, Argentina. Revista Brasileira de Entomologia 55: 454-456.

De Bortoli SA, Pplanczyk RA, Vacari AM, De Bortoli CP Duarte RT 2014. *Plutella xylostella* (Lnnaeus, 1758) (Lepidoptera, Plutellidae): Tactics for intigrated pest management in Brassicaceae. Intech, pp. 31-51.

Hagerty AM, Pantoja A Emmert S 2008. First record of diamondback moth (Lepidoptera: Plutellidae) from interior Alaska. Western North American Naturalist 68: 249-250.

Happner JB 2008. Diamondback moths (Lepidoptera: Plutellidae). Encyclopedia of Entomolog: Capinera J. L. (Ed.), pp. 1206-2109.

Karsholt O, Razowski J 1996. The Lepidoptera of Europe: a distributional checklist. Brill Academic Pub. 380 p.

Koçak AÖ, Kemal M 2006. Checklist of the Lepidoptera of Turkey. Centre for Entom Studies.

Koçak A, Kemal M 2007. Revised and annotated checklist of the Lepidoptera of Turkey. Priamus. Serial Publication of the Centre for Entom Studies Ankara 8: 26-42.

Koçak AÖ, Kemal M 2009. Revised checklist of the Lepidoptera of Turkey. Centre for Entom Studies Ankara 17: 1-150.

Koçak AÖ, Kemal M 2018. A synonymous and distributional list of the species of the Lepidoptera of Turkey. Centre for Entom Studies Ankara 8: 1-489.

Moriuti S 1986. Taxonomic notes on the Diamondback moth. Asian Vegetable Research and Development Center: pp. 83-88.

Pengyan L, Junwei Z, Qin Y 2012. Enhanced attraction of *Plutella xylostella* (Lepidoptera: Plutellidae) to pheromone-baited traps with the addition of green leaf volatiles. J of Economic Ento 105: 1149-1156.

Robinson GS, Sattler K 2001. Plutella in the Hawaiian Islands: Relatives and host-races of the diamondback moth (Lepidoptera: Plutellidae). Bioshop Museum Occasional Papers: pp. 67, 1-27.

Eurasian J. Bio. Chem. Sci. 2(1): 11-16

EJBCS

Eurasian Journal of Biological and Chemical Sciences

Journal homepage: www.dergipark.org.tr/ejbcs

Farklı ışık yayan diyotlar (LED) altında tıbbi sucul bitki *Lysimachia nummularia* L.'nın boğum eksplantlarından çoklu sürgün rejenerasyonu

Muhammet Dogan *

*Karamanoğlu Mehmetbey Üniversitesi, Kamil Özdağ Fen Fakültesi, Biyoloji Bölümü, Karaman, Türkiye

*Corresponding author : mtdogan1@gmail.com
Orcid No: 0000-0003-3138-5903

Received : 12/05/2019
Accepted : 05/06/2019

Özet: Bitki büyüme ve gelişimi için önemli avantajlara sahip Işık yayan diyotlar (LED) doku kültürü çalışmalarında kullanılmaya başlanmıştır. LED'lerin ışık renkleri bitkiler üzerinde farklı etkiler göstermektedir. Bu çalışmada, beyaz (B), kirmizi (K), mavi (M) LED ışıkların *Lysimachia nummularia* L.'nın çoklu sürgün rejenerasyonu üzerine tek ve kombine etkileri incelenmiştir. Boğum eksplantları 0,10 mg/L indol butirik asit (IBA) ve 0,20-0,80 mg/L Thidiazuron (TDZ) eklenmiş Murashige ve Skoog (MS) besin ortamında sekiz hafta süre ile kültüre edilmiştir. Her üç hormon uygulamasında %100 sürgün rejenerasyon frekansları 2B:1K:1M ve 1B:1K:1M LED ışıkları altında kaydedilmiştir. En fazla sürgün sayısı 1B:2K:1M LED ışıklar altında sırasıyla 17,47, 16,16 ve 13,46 adet olarak 0,40 mg/L TDZ + 0,10 mg/L IBA, 0,20 mg/L TDZ + 0,10 mg/L IBA ve 0,80 mg/L TDZ + 0,10 mg/L IBA eklenmiş MS besin ortamında belirlenmiştir. En az sayıda sürgünler ise mavi LED altında kaydedilmiştir. En uzun sürgünler tüm ortamlarda 1B:1K:2M LED ışık altındaki eksplantlardan elde edilmiştir. TDZ'nin kültür ortamında fazla kullanılması sürgün uzunluğunu olumsuz etkilemiştir. Çoğaltım denemelerinde yoğun kök oluştuğundan dolayı ayrıca köklendirme yapılmamıştır. Kültür ortamında üretilen bitkiler dış koşullara başarıyla alıştırılmıştır. Sonuç olarak çalışma, LED ışıkların *L. nummularia*'nın üretimindeki etkinliğini ve flouresan ışıklara göre üstünlüğünü göstermiştir.

Anahtar Kelimeler: Doku kültürü, Işık etkisi, LED, Shoot rejenerasyonu

Multiple shoot regeneration from nodal explants of medicinal aquatic plant Lysimachia nummularia L. under different light emitting diodes (LEDs)

Abstract: Light emitting diodes (LEDs), which have important advantages for plant growth and development, have been used in tissue culture studies. The light colours of LEDs show different effects on plants. In this study, single and combined effects of white (W), red (R), blue (B) LED lights on multiple shoot regeneration of *Lysimachia nummularia* L. were investigated. Nodal explants were cultured for eight weeks in a Murashige and Skoog (MS) nutrient medium supplemented with 0.10 mg/L indole butyric acid (IBA) and 0.20-0.80 mg/L Thidiazuron (TDZ). 100% shoot regeneration frequencies in all three hormone applications were recorded under 2W:1R: 1B and 1W: 1R: 1B LED lights. The maximum number of shoots was determined under 1W:2R:1B LED lights as 17.47, 16.16 and 13.46 shoots/explant in the MS nutrient medium added 0.40 mg/L TDZ + 0.10 mg/L IBA, 0.20 mg/L TDZ + 0.10 mg/L and 0.80 mg/L TDZ + 0.10 mg/L IBA, respectively. The minimum number of shoots was recorded under blue LED. The longest shoot was obtained from explants under 1W:1R:2B LED light in all environments. Excessive use of TDZ in the culture medium adversely affected shoot length. Since there was a dense root in replication experiments, no rooting was performed. Plants produced in the culture environment have been successfully adapted to external conditions. As a result, the study showed the effectiveness of the LED lights on the production of *L. nummularia* and their superiority over the fluorescent lights.

Keywords: Tissue culture, Light effect, LED, Shoot regeneration

1. Giriş

Işık yayan diyotlar (LED) ile ilk bitki üretimi çalışmalarının çoğu, NASA'ya bağlı araştırmacılar tarafından bitki bazlı rejeneratif yaşam destek sistemlerinin geliştirilmesine hazırlık olarak yürütülmüştür. Günümüzde LED'ler, bahçecilik ve seracılıkta kullanılan gaz halindeki deşarj tipi lambalardan farklı bir teknolojiyi temsil etmektedir. Spektral kompozisyon kontrolü ve az radyant ısıyla yüksek ışık çıkışı gibi özellikleri ile LED'ler, bahçecilik ve seracılıkta bitki üretimi için en önemli gelişmelerden biri haline getirmiştir (Morrow, 2008).

LED'ler, floresan ve akkor lambalardan elektrik enerjisi başına daha fazla ışık üretir. Herhangi bir lambadan çok daha sağlamdır ve floresan lambalar gibi tehlikeli madde içermeyen katı hal cihazlardır. LED'ler akkor ve floresan

lambalardan çok daha uzun bir ömre sahiptir (Bourget, 2008).

LED tabanlı aydınlatma sistemleri, özellikle bahçecilikte birçok avanta sağlamaktadır. Birincisi, geniş spektrumlu kaynaklarla kolayca yapılamayan bir aydınlatma sisteminin spektral çıktısını kontrol etme yeteneğidir. LED'ler, belirli ışık renklerinin yanı sıra, istenen yönde yüksek düzeyde ışık yayabilir. Bitkisel üretimde kullanılan diğer ışık kaynaklarında istenmeyen renkler filtrelenerek boşa enerji harcar. LED'lerde saf renkli ışıkları filtrelenmeden üretilir (Dănilă ve Lucache, 2013: Dougher ve Bugbee, 2001). Spektral çıktının dinamik olarak kontrol edilebilmesi, bitki morfolojisini etkilemek için de kullanılabilir (Heo ve ark., 2002).

Doku kültürü teknikleri bitki üretimi için önemli bir alternatiftir. Son yıllarda bu tekniği kullanarak *Ceratophyllum demersum* L. (Emsen ve Dogan, 2018; Dogan, 2019a), *Plumbago zeylanica* L. (Sharma ve Agrawal, 2018), *Bacopa monnieri* L. Pennell (Dogan ve Emsen, 2018) *Rotala rotundifolia* (Buch-Ham. ex Roxb) Koehne (Dogan, 2019b), *Fagraea fragrans* Roxb (Fatonah ve Isda, 2018) ve *Pogostemon erectus* (Dalzell) Kuntze (Dogan, 2019c) gibi birçok bitkinin etkili ve hızlı çoğaltımı başarılmıştır. Bu çalışmada, doku kültürü koşullarında farklı LED ışıkları altında *Lysimachia nummularia* L.'nın üretimi hedeflenmiştir. Bu bağlamda, beyaz, kırmızı ve mavi LED ışıkların *L. nummularia*'nın çoklu sürgün rejenerasyonu üzerine tek ve birlikte etkileri incelenmiştir.

2. Materyal ve Metot

Bitki materyali olarak *L. nummularia* kullanılmıştır. Bu bitkiler Konya-Türkiye'deki akvaryumculardan temin edilmiştir. Bitkiler, yüzey sterilizasyonundan önce akan musluk suyu altında bekletilmiştir. *L. nummularia*'nın yüzey sterilizasyonu, 10 dk boyunca ticari çamaşır suyu (NaOCI) ile işlemden geçirilerek elde edilmiştir. 5'er dk x 3 defa durulamadan sonra, boğum eksplantları izole edilmiştir. Eksplantlar daha sonra bitki büyüme düzenleyici içermeyen Murashige ve Skoog (MS) ortama aktarılmıştır (Murashige ve Skoog, 1962). Deneylerde, bu kültür ortamında geliştirilen dört haftalık boğum eksplantları kullanılmıştır.

Doku kültürü çalışmalarında MS mineral tuzu ve vitaminleri içeren temel besin ortamı ile %3 sukroz (Duchefa) ve % 0,65 agar (Duchefa) kullanılmıştır. Ortam hazırlığında ultra saf su kullanılmıştır. MS besin ortamına 0,10 mg/L indol butirik asit (IBA) ve 0,20, 0,40 ve 0,80 mg/L Thidiazuron (TDZ) ilave edilmiştir. Besiyerinin pH'ı, 1N NaOH ve 1N HCI kullanılarak 5.7 ± 0.1'e ayarlanmıştır. 1.2 atmosferik basınç altında ve 120°C'de 20 dk süre ile otoklavda sterilizasyon işlemi gerçekleştirilmiştir.

L. nummularia'nın *in vitro* rejenerasyon için boğum eksplantları, yedi farklı LED ve beyaz floresan ışığı altında sekiz hafta boyunca kültüre edilmiştir. Kullanılan LED ışıklar, beyaz (B), kirmizi (K), mavi (M) ve bunların farklı oranlardaki kombinasyonlarıdır (Tablo 1). Ek olarak, kontrol amacıyla beyaz floresan ışık kullanılmıştır. LED ışık odasına yerleştirilen kültürlerin ışık koşulları 16 saat aydınlık ve 8 saat karanlık olarak belirlenmiştir. Denemelerde, tüm ışık yoğunlukları 1500 lux'de (24°C) sabit tutulmuştur. Bu çalışmalar çoklu sürgün rejenerasyonu için en etkili ışık ortamını belirlemeyi amaçlamıştır.

Tablo 1. *In vitro* sürgün rejenerasyonu için kullanılan farklı ışık uygulamaları

Işık uygulamaları
2 Beyaz LED :1 Kırmızı LED :1 Mavi LED (2B:1K:1M)
1 Beyaz LED :2 Kırmızı LED :1 Mavi LED (1B:2K:1M)
1 Beyaz LED :1 Kırmızı LED :2 Mavi LED (1B:1K:2M)
1 Beyaz LED :1 Kırmızı LED :1 Mavi LED (1B:1K:1M)
Beyaz LED
Kırmızı LED
Mavi LED
Beyaz flouresan ışık

Çoğaltım ortamlarında sürgünlerden çok sayıda kök çıkması nedeniyle ayrıca köklendirme çalışması uygulanmamıştır. Bitkiler daha sonra çevre şartlarına alışmak için cam akvaryuma transfer edilmiştir. Akvaryum zeminine yüksekliği 4-5 cm olan nehir kumu yerleştirilmiştir. Akvaryumun içine 16 saat ışık verilmiş (1500 lüks) ve sıcaklık 24ºC ayarlanmıştır.

Denemeler 6 tekrarlı olarak gerçekleştirilmiştir. SPSS 16 for Windows programı ile veriler analiz edilmiştir. Post Hoc analizleri için Duncan testinden yararlanılmıştır. Yüzde veriler arksin dönüşümüne çevrilmiştir (Snedecor ve Cochran, 1997).

3. Bulgular ve Tartışma

Çoklu bitki üretimi için *L. nummularia*'nın boğum eksplantları 0,10 mg/L IBA ve 0,20-0,80 mg/L TDZ ilave edilmiş kültür ortamında, farklı ışıklar altında kültüre edilmiştir. İki hafta sonunda ışık ortamlarında sürgün uçları belirmeye başlamıştır. Sekiz hafta sonunda deneme sonuçlandırılmış ve sürgün rejenerasyon değerleri Tablo 2'de gösterilmiştir. Bitki doku kültürü çalışmalarında eksplant çeşidi oldukça önemlidir. Boğum eksplantları doku kültürü denemelerinde birçok araştırmacı tarafından kullanılmıştır (Venkatachalam ve ark., 2017; Rameshkumar ve ark., 2017; Acemi ve ark., 2018; Dogan 2018a, 2018b; Najar ve ark., 2018).

Faklı LED ışıkları ve beyaz flouresan ışık ortamları ile yapılan çalışmada sürgün rejenerasyon oranı 0,20 mg/L TDZ + 0,10 mg/L IBA içeren kültürlerde %72,22-100, 0,40 mg/L TDZ + 0,10 mg/L IBA içeren kültürlerde %61,11-100 ve 0,80 mg/L TDZ + 0,10 mg/L IBA içeren kültürlerde %66,66-100 arasında değişmiştir (Tablo 2).

Tablo 2. Farklı ışık ortamlarının *L. nummularia'*nın boğum eksplantlarından sürgün rejenerasyon oranına etkisi

Işık Ortamları	Büyüme Düzenleyicileri		
	0,20 mg/L TDZ + 0,10 mg/L IBA**	**0,40 mg/L TDZ + 0,10 mg/L IBA***	**0,80 mg/L TDZ + 0,10 mg/L IBA****
2B:1K:1M	100,00[a]	100,00[a]	100,00[a]
1B:2K:1M	100,00[a]	94,44[ab]	94,44[a]
1B:1K:2M	100,00[a]	94,44[ab]	83,33[ab]
1B:1K:1M	100,00[a]	100,00[a]	100,00[a]
Beyaz LED	77,77[ab]	88,89[ab]	94,44[a]
Kırmızı LED	72,22[b]	72,22[bc]	66,66[b]
Mavi LED	77,77[ab]	72,22[bc]	77,77[ab]
Beyaz Işık Flouresan	83,33[ab]	61,11[c]	83,33[ab]

**Aynı sütunda farklı harfler $p<0,01$ seviyesinde anlamlıdır.
* Aynı sütunda farklı harfler $p<0,05$ seviyesinde anlamlıdır.
B: Beyaz LED ışık, K: Kırımız LED ışık, M: Mavi LED ışık

0,20 mg/L TDZ + 0,10 mg/L IBA içeren MS ortamında beyaz, kırmızı ve mavi LED ışık kombinasyonlarında %100 sürgün rejenerasyonu elde edilirken, 0,40 ve 0,80 mg/L TDZ + 0,10 IBA içeren MS ortamında ise 2B:1K:1M ve 1B:1K:1M ışık ortamlarında %100,00 sürgün rejenerasyonu elde edilmiştir. En düşük sürgün rejenerasyon oranı 0,20 ve 0,80 mg/L TDZ + 0,10 mg/L IBA içeren kültürlerde kırmızı LED ışık altındaki kültür ortamlarında belirlenirken, 0,80 mg/L TDZ + 0,10 mg/L IBA eklenmiş kültürlerde beyaz flouresan ışık altında belirlenmiştir. Genel olarak beyaz, kırmızı ve mavi LED ışıkların birlikte verildiği eksplantlarda sürgün rejenerasyon oranı yüksek çıkmıştır.

Tablo 3. Farklı ışık ortamlarının *L. nummularia'*nın boğum eksplantlarından eksplant başına sürgün sayısına etkisi

Işık Ortamları	Büyüme Düzenleyicileri		
	0,20 mg/L TDZ + 0,10 mg/L IBA**	**0,40 mg/L TDZ + 0,10 mg/L IBA****	**0,80 mg/L TDZ + 0,10 mg/L IBA***
2B:1K:1M	13,6[6ab]	16,05[ab]	11,77[ab]
1B:2K:1M	16,16[a]	17,47[a]	13,46[a]
1B:1K:2M	11,27[bc]	12,287[abc]	8,35[bc]
1B:1K:1M	12,27[ab]	14,77[ab]	11,16[ab]
Beyaz LED	11,08[bc]	14,39[ab]	9,47[abc]
Kırmızı LED	8,05[cd]	7,33[c]	7,11[bc]
Mavi LED	5,66[d]	6,19[c]	5,33[c]
Beyaz Işık Flouresan	8,30[cd]	10,19[bc]	7,64[bc]

**Aynı sütunda farklı harfler $p<0,01$ seviyesinde anlamlıdır.
* Aynı sütunda farklı harfler $p<0,05$ seviyesinde anlamlıdır.
B: Beyaz LED ışık, K: Kırımız LED ışık, M: Mavi LED ışık

Boğum eksplantlarının kullanıldığı kültür ortamlarında eksplant başına sürgün sayısı 0,20, 0,40, 0,80 mg/L TDZ ve 0,10 mg/L IBA eklenmiş kültürlerde sırasıyla 5,66-16,16, 6,19-17,47 ve 5,33-13,46 adet olarak belirlenmiştir (Tablo 3). En fazla sürgün sayısı kombinasyon şeklinde kullanılan LED ışıklar altında ve kırmızı LED'in mavi ve beyaz LED ışık oranına göre iki kat daha yoğun olduğu ışık altında (1B:2K:1M) sırasıyla 17,47 adet ile 0,40 mg/L TDZ + 0,10 mg/L IBA eklenmiş MS besin ortamında (Şekil 1a), 16,16 adet ile 0,20 mg/L TDZ + 0,10 mg/L IBA eklenmiş MS besin ortamında (Şekil 1b) ve 13,46 adet ile 0,80 mg/L TDZ + 0,10 mg/L IBA eklenmiş MS besin ortamında (Şekil 1c) elde edilmiştir. Benzer şekilde, LED ışıkları kullanılarak doku kültürü koşullarında çoklu sürgünler daha önce *Lysionotus pauciflorus* maxim. (Lu ve ark., 2013), *Lactuca sativa* L. var. capitata (Lin ve ark., 2013) ve *Curculigo orchioides* Gaertn (Gupta ve Sahoo, 2015) bitkilerinde de bildirilmiştir.

En az sürgün sayısı ise mavi LED ışık altında sırasıyla 5,33, 5,66 ve 6,19 adet olarak sırasıyla 0,80 mg/L TDZ + 0,10 mg/L IBA'lı, 0,20 mg/L TDZ + 0,10 mg/L IBA'lı ve 0,40 mg/L TDZ + 0,10 mg/L IBA'lı kültürlerde kaydedilmiştir. Genel olarak sürgün sayısı bakımından kombinasyon şeklinde kullanılan LED ışıklar, tek olarak kullanılan LED ışıklara kıyasla daha etkili bulunmuştur.

Kültür ortamlarında sürgün uzunlukları 0,20, 0,40 ve 0,80 mg/L TDZ + 0,10 mg/L IBA içeren MS ortamında sırasıyla 0,84-1,76 cm, 0,68-1,49 cm ve 0,61-1,37 cm arasında kaydedilmiştir (Tablo 4). En uzun sürgünler tüm ortamlarda 1B:1K:2M LED ışık altında ardında ise 1B:1K:1M LED ışık altındaki eksplantlardan elde edilmiştir. Tüm kültür ortamlarında en uzun sürgünler sırasıyla TDZ'nin 0,20, 0,40 ve 0,80 mg/L kullanıldığı besin ortamında elde edilmiştir. Kullanılan TDZ konsantrasyonu arttıkça sürgün uzunluğu kısalmıştır. Bu bulgular ile benzer şekilde TDZ'nin sürgün uzunluğu üzerine olumsuz etkisi daha önce Debnath (2005), Ledbetter ve Preece (2004) ve Tomson eve ark. (2004) tarafından da bildirilmiştir.

En kısa sürgünler ise her üç hormon oranında da mavi LED altındaki eksplantlardan tespit edilmiştir. Sonuç olarak, *L. nummularia*'nın boğum eksplantından en uzun sürgünler 0,20 mg/L TDZ + 0,10 mg/L IBA içeren MS ortamında ve 1B:1K:2M LED ışık ortamındaki elde edilmiştir. Tekli LED ışıklar genel kombinasyon şeklinde kullanılan LED'lere göre daha düşük sonuçlar vermiştir.

In vitro üretim denemelerinde sürgünlerden çok sayıda kök oluşmuştur. Bu nedenle ayrıca köklendirme çalışması yapılmamıştır. Bitkiler daha sonra dış koşullara alışmak için akvaryum ortamına aktarılmış ve dört hafta sonunda bitkilerin alıştırılması başarıyla sağlanmıştır.

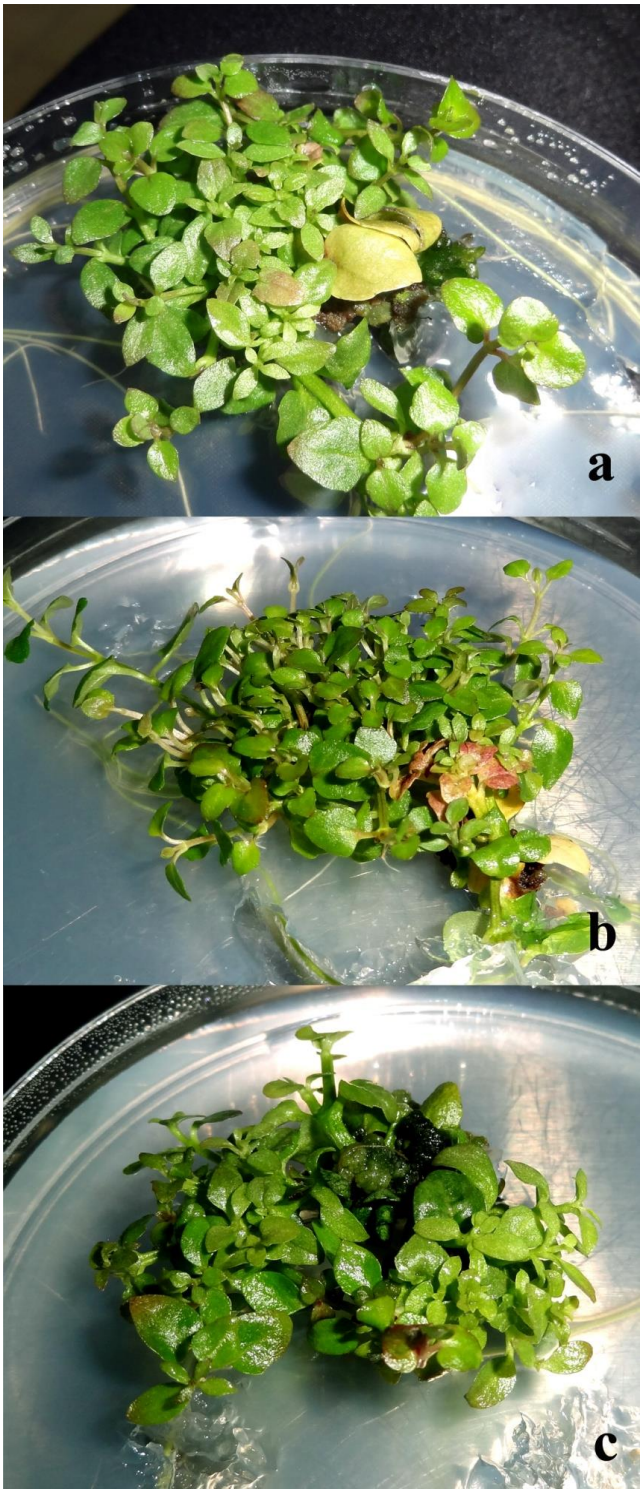

Şekil 1. 1B:2K:1M LED ışık ortamı altında **a)** 0,20 mg/L TDZ + 0,10 mg/L IBA **b)** 0,40 mg/L TDZ + 0,10 mg/L IBA ve **c)** 0,80 mg/L TDZ + 0,10 mg/L IBA eklenmiş kültür ortamında *L. nummularia*'nın boğum eksplantlarından sürgün rejenerasyonu

Tablo 4. Farklı ışık ortamlarının *L. nummularia*'nın boğum eksplantlarından sürgün uzunluğuna etkisi

Işık Ortamları	Büyüme Düzenleyicileri		
	0,20 mg/L TDZ + 0,10 mg/L IBA	**0,40 mg/L TDZ + 0,10 mg/L IBA**	**0,80 mg/L TDZ + 0,10 mg/L IBA**
2B:1K:1M	1,24^{bc}	1,09^{bc}	0,84^{cde}
1B:2K:1M	1,28^{bc}	1,17^{b}	0,97^{bcd}
1B:1K:2M	1,76^{a}	1,49^{a}	1,37^{a}
1B:1K:1M	1,46^{ab}	1,34^{ab}	1,12^{b}
Beyaz LED	1,15b^{cd}	1,11^{bc}	1,04^{bc}
Kırmızı LED	0,93^{cd}	0,85^{cd}	0,76^{def}
Mavi LED	0,84^{d}	0,68^{d}	0,61^{f}
Beyaz Işık Flouresan	0,91^{cd}	0,74^{d}	0,65^{ef}

**Aynı sütunda farklı harfler $p<0,01$ seviyesinde anlamlıdır.
* Aynı sütunda farklı harfler $p<0,05$ seviyesinde anlamlıdır.
B: Beyaz LED ışık, K: Kırımız LED ışık, M: Mavi LED ışık

Sonuç

Doku kültürü ve bahçecilik alanlarında LED aydınlatmalar parlak bir geleceğe sahiptir. Enerji verimliliği, uzun ömür ve uygulama esnekliği, LED'leri gelecekteki tarımsal aydınlatma sistemleri için doğal bir seçim haline getirmektedir. Bu bağlamda, beyaz, kırmızı ve mavi LED ışıkların tekli ve kombinasyon halleri *L. nummularia*'nın *in vitro* üretimi için test edilmiş ve çoklu sürgünler başarıyla elde edilmiştir. En etkili LED ışık 1B:2K:1M LED'ler olarak belirlenmiştir. Genel olarak kombinasyon halinde kullanılan LED ışıklar, tekli LED ışıklara göre daha iyi sonuçlar vermiştir. Bu çalışma sonuçları itibariyle LED ışıkların flouresan ışıklara göre daha etkili olduğu öne sürülebilir.

Teşekkür

Bu çalışma, Türkiye Bilimsel ve Teknolojik Araştırma Kurumu (TÜBİTAK) tarafından desteklenmiştir (Proje no:2130190).

Kaynaklar

Acemi A, Bayrak B, Çakır M, Demiryürek E, Gün E, El Gueddari NE, Özen F 2018. Comparative analysis of the effects of chitosan and common plant growth regulators on *in vitro* propagation of *Ipomoea purpurea* (L.) Roth from nodal explants. *In Vitro* Cell Dev Biol Plant 54(5): 537-544.

Bourget CM 2008. An introduction to light-emitting diodes. HortScience 43(7): 1944-1946.

Dănilă E, Lucache DD 2013. Cost effectiveness of growing plant lighting system. Journal of Electrical Engineering 13(4): 224-229.

Debnath SC 2005. Micropropagation of lingonberry: influence of genotype, explant orientation, and overcoming TDZ-induced inhibition of shoot elongation using zeatin. HortScience 40(1): 185-188.

Dogan M 2018a. *In vitro* shoot regeneration of *Limnophila aromatica* (Lamk.) Merr. from nodal and internodal explants. Iğdır Univ J Inst Sci & Tech 8: 77-84.

Dogan M 2019a. Multiple shoot regeneration via indirect organogenesis from shoot tip and nodal meristem explants of *Ceratophyllum demersum* L. J Anim Plant Sci 29: 568-577.

Dogan M 2019b. Callus formation from full leaf and leaf parts of *Rotala rotundifolia* (Buch-Ham. ex Roxb) Koehne. Acta Biologica Turcica 32: 78-83.

Dogan M 2019c. *In vitro* rapid propagation of an aquatic plant *Pogostemon erectus* (Dalzell) Kuntze. Ant J Bot 3: 1-6.

Dogan M 2018b. *In vitro* micropropagation from nodal explants of the medicinal plant *Lysimachia nummularia* L.. KSU J Agric Nat 21(6): 875-881.

Dogan M, Emsen B 2018. Anti-cytotoxic-genotoxic influences of *in vitro* propagated *Bacopa monnieri* L. Pennell in cultured human lymphocytes. Eurasian J Bio Chem Sci 1(2): 48-53.

Dougher T, Bugbee B 2001. Differences in the response of wheat, soybean and lettuce to reduced blue radiation. Photochem Photobiol 73: 199- 207.

Emsen B, Dogan M 2018. Evaluation of antioxidant activity of *in vitro* propagated medicinal *Ceratophyllum demersum* L. extracts. Acta Sci Pol-Hortoru 17: 23-33.

Fatonah S, Isda MN 2018. *In vitro* shoot regeneration of tembesu (*Fagraea fragrans* Roxb.) from seed explants

on different concentrations of sucrose and honey. Biosci Res 15(2): 655-662.

Gupta SD, Sahoo TK 2015. Light emitting diode (LED)-induced alteration of oxidative events during *in vitro* shoot organogenesis of *Curculigo orchioides* Gaertn. Acta Physiol Plant 37(11): 233.

Heo J, Lee C, Chakrabarty D, Paek K 2002. Growth responses of marigold and salvia bedding plants as affected by monochromic or mixture radiation provided by a light-emitting diode (LED). Plant Growth Regulat 38: 225-230.

Ledbetter DI, Preece JE 200). Thidiazuron stimulates adventitious shoot production from *Hydrangea quercifolia* Bartr. leaf explants. Sci Hort 101(1-2): 121-126.

Lin KH, Huang MY, Huang WD, Hsu MH, Yang ZW, Yang CM. 2013. The effects of red, blue, and white light-emitting diodes on the growth, development, and edible quality of hydroponically grown lettuce (*Lactuca sativa* L. var. capitata), Sci Hort 150: 86-91.

Lu YX, Godo T, Fujiwara K, Guan KY, Mii M 2013. Effects of nitrogen source and wavelength of led-light on organogenesis from leaf and shoot tip cultures in *Lysionotus pauciflorus* maxim. Propag Ornam Plants 13: 174-180.

Morrow RC 2008. LED lighting in horticulture. HortScience 43(7): 1947-1950.

Murashige T, Skoog F 1962. A revised medium for rapid growth and bioassays with tobacco tissue cultures. Physiol Plant 15: 473-497.

Najar RA, Fayaz M, Bhat MH, Bashir M, Kumar A, Jain AK 2018. An efficient micropropagation protocol for direct organogenesis from nodal explants of medicinal climber, *Tylophora indica*. Biosci Biotech Res Comm 11(1): 144-153.

Rameshkumar R, Largia MJV, Satish L, Shilpha J, Ramesh M 2017. *In vitro* mass propagation and conservation of *Nilgirianthus ciliatus* through nodal explants: A globally endangered, high trade medicinal plant of Western Ghats. Plant Biosyst 151(2): 204-211.

Sharma U, Agrawal V 2018. *In vitro* shoot regeneration and enhanced synthesis of plumbagin in root callus of *Plumbago zeylanica* L.-an important medicinal herb. *In Vitro* Cell Dev Biol Plant 54(4): 423-435.

Snedecor GW, Cochran WG 1997.Statistical methods. Iowa, USA: The Iowa State University Press, USA.

Tomsone S, Gertnere D, Novikova D 2004. The influence of thidiazuron on shoot regeneration and proliferation of rhododendrons *in vitro*. Acta Univ Latv 676: 239-242.

Venkatachalam P, Jinu U, Gomathi M, Mahendran D, Ahmad N, Geetha N, Sahi SV 2017. Role of silver nitrate in plant regeneration from cotyledonary nodal segment explants of *Prosopis cineraria* (L.) Druce.: A recalcitrant medicinal leguminous tree. Biocatal Agric Biotechnol 12: 286-291.

Eurasian J. Bio. Chem. Sci. 2(1): 17-23

EJBCS

Eurasian Journal of Biological and Chemical Sciences

Journal homepage: www.dergipark.org.tr/ejbcs

Beta Glucosidase Recognition By Imprinted Polyacrylamide Hydrogels

Mervecan Sevildik[1], Ayşe Dinçer [1*], Tülin Aydemir [1]

[1] *Manisa Celal Bayar University, Faculty of Science and Arts, Chemistry Department, Manisa, Türkiye.*

*Corresponding author : ayse.dincer@cbu.edu.tr
Orcid No: 0000-0001-6158-1775

Received : 04/01/2019
Accepted : 30/09/2018

Abstract: In the present work, selective adsorption of β-glucosidase using imprinted polyacrylamide hydrogels were studied. For this purpose imprinted hydrogels were prepared using β-glucosidase as a template molecule, acrylamide (AAm) as a monomer, N,N'-methylenebisacrylamide (MBAA) as a crosslinker, ammonium persulphate (APS) and N,N,N',N'-tetramethylethylene-diamine (TEMED) as initiators. β-Glucosidase imprinted hydrogel was washed with a solution of sodium dodecyl sulfate (SDS) and acetic acid to remove the template molecule. Non-imprinted hydrogel was also prepared without using β-glucosidase template. The adsorption and recognition performance of hydrogels towards β-glucosidase was discussed through adsorption isotherms and adsorption kinetics. In batch template rebinding experiments, imprinted hydrogels displayed quite high template binding capacity than non-imprinted hydrogels. The theoretical maximum adsorption capacity (Qmax) was determined by the Langmuir model, which turned out to be 7.2 mg/g and 4.6 mg/g for imprinted and non-imprinted hydrogels, respectively. A pseudo-second-order model was suitable to interpret kinetic data. Imprinted polyacrylamide hydrogels also used as an affinity sorbent for selective β-glucosidase adsorption from almonds.

Keywords: β-Glucosidase, polyacrylamide, hydrogel, molecular imprinting.

1. Introduction

Molecular imprinting is regarded as a promising technique for preparing artificial receptors with "tailor-made"-binding sites for specific binding the template molecular by polymerizing a mixture of appropriate functional monomer, befitting cross-linker and template. (Zhao et al. 2014, Pisarev and Polyakova 2018, Wang et al. 2018) Molecularly imprinted polymers (MIPs) are characterized by their thermal and chemical stability, high specificity, ease of mass preparation, low cost and reusability, which promote their wide applications in chromatography, catalysis, sensors, drug release and environmental protection. (Zaidi 2018, Li et al. 2005) There are several challenges remain in bio-macromolecule imprinting, such as those involving proteins, DNAs, and even whole cells and viruses. Many inherent problems of bio-macromolecules hinder the advancement of their imprinting, such as large molecular size, structural complexity, environmental sensitivity, and flexible conformation (Nishino et al. 2006, Lv et al, 2013). The use of hydrogel with soft and macroporous structure is beneficial in maintaining the native protein conformation. Imprinting within hydrogels presents the possibility of three dimensional binding sites that eventually should lead to improved selectivity, while imprinting in an aqueous phase ensures solubility and conformational stability of the template proteins (Kimhi and Bianco-Peled, 2007).

Polyacrylamide (PAM) hydrogel was widely used as the matrix for the molecular imprinting of proteins. PAM hydrogel is biocompatible and has soft and wet macroporous structure. The abundant amide functional groups in PAM can form strong interactions with peptide bonds in the proteins even in aqueous system (Zhao et al. 2015). β-Glucosidase (EC 3.2.1.21) is a type of hydrolase widely existing in various sources such as microorganisms, plant and animal tissues. It catalyzes the hydrolysis of β-glycosidic linkages in di- and oligoglucosaccharides and several other glycol conjugates (Verma et al. 2011, Çelik et al. 2016). In this study, imprinted polyacrylamide hydrogels for recognition of β-glucosidase were prepared and tested for β-glucosidase rebinding. Effect of contact time, pH, temperature, initial β-glucosidase concentration on rebinding of β-glucosidase on MIP and NIP hydrogels were investigated. To investigate the nature of the adsorption process, the non-linear Langmuir and Freundlich isotherms were used to fit the equilibrium adsorption data.The kinetic data have been analyzed using a pseudo-first-order, pseudo-second-order equations. β-glucosidase imprinted polyacrylamide hydrogels also used as an affinity matrix for selective adsorption of the enzyme from almonds. Purity controls were done using SDS-PAGE.

2. MATERIALS AND METHOD

2.1 Materials

β-glucosidase from almonds (≥2 U/mg solid), acrylamide (AAm), N,N'-methylene bisacrylamide (MBA), ammonium persulfate and N,N,N',N'-tetramethylethylene-diamine (TEMED) were supplied from Sigma-Aldrich.

All other chemicals used in this study were in analytical grade.

2.2 Method

2.2.1 Preparation of β-glucosidase imprinted hydrogel

Molecularly imprinted hydrogels (MIP) were synthesized by dissolving AAm (54 mg), and MBA as a crosslinker (6 mg), respectively along with template protein β-glucosidase (10 mg) in 1 mL of phosphate buffer (0.1 M, pH 7.0). The prepolymerization solution was purged with nitrogen gas for 10 min. to remove dissolved oxygen followed by an addition of 10 mg APS and 20 µL of a 5% (v/v) TEMED solution. Polymerization occurred overnight at room temperature. The template molecule β-glucosidase was eluted from hydrogel with acetic acid solution (10%, v/v) containing SDS (10%, w/v) until no protein in the supernatant was detected. Protein measurements were done by Bradford method. Ultimately, the hydrogel was extensively washed with deionized water to remove remnant SDS and acetic acid. Non-imprinted hydrogel (NIP) was also prepared, which corresponds to imprinted hydrogel (MIP) but without the template. All the MIP and NIP hydrogels were dried at 50 °C for 12 h before use.

2.2.2 Adsorption studies

β-glucosidase rebinding onto imprinted and non-imprinted hydrogels were carried out using a batchwise adsorption method. In each rebinding experiments, enzyme solution (1 mL) prepared in buffer and 0.01 g of dried imprinted and non-imprinted hydrogels were used. The experiments were conducted to observe the effect of various parameters such as contact time, temperature, pH and enzyme concentration. The effect of contact time on β-glucosidase adsorption was studied by varying the contact time from 15 to 120 min. The effect of the temperature on the adsorption was studied at various temperature values (25-40°C) accompanied by mild shaking. Effect of enzyme concentration on the adsorption was also recorded in the concentration range from 1-3.5 mg/mL. After adsorption, the hydrogels were removed by centrifugation and the supernatant was analyzed for the unadsorbed enzyme spectrophotometrically.
The amount of enzyme adsorbed on the hydrogels were calculated according to the following equation 1:

$$qe = \frac{(C_0.V_0 - Ce.V)}{m} \qquad (1)$$

where qe is the amount of protein adsorbed onto unit mass of dry gel (mg/g), C_0 and Ce are the initial and equilibrium concentrations of protein (mg/mL), respectively, V_0 and V is volume (mL) of the initial and final enzyme solution containing the hydrogel and m is the amount of dry hydrogel (g) used in the experiment (Bhattacharyya and Ray 2013).

The specific recognition property of the imprinted hydrogel is illustrated by the imprinting factor (IF) according to the Kempe and Mosbach 1994, which is defined as:

$$IF = \frac{q_{imprinted}}{q_{nonimprinted}} \qquad (2)$$

where $q_{imprinted}$ is the amount of protein on the imprinted hydrogel (mg/g), and $q_{non\text{-}imprinted}$ is the amount of protein on the non-imprinted hydrogel (mg/g).

2.2.3 Partial purification of β-glucosidase from almonds

Partial purification of β-glucosidase from almonds was done according to the method of Ergöçen (2013). In brief, 8 mL of chilled acetone (-20 °C) was added to each gram of almonds extracted from hard shells and homogenized in porcelain mortar. By filtering the homogenate through filter paper, the phenolic compounds and some lipids were removed together with the filtrate. The remaining portion of the sample on filter paper was taken back to the porcelain mortar and the process was repeated 3 times as described above. As a result of the final filtration, the remaining solid in the filter paper was stored at 5 °C for 24 hours to evaporate acetone. 1 g of the solid extract obtained after acetone extraction was dissolved in 50 mL of citric acid (50 mM, pH 5) buffer and 60% $(NH_4)_2SO_4$ precipitation was applied. The precipitate obtained after the ammonium sulfate precipitation was suspended in 50 mM pH 5.0 citrate buffer (4 mL) and dialyzed. The dialyzed enzyme solution applied on MIP and NIP hydrogels and incubated for 120 min. Recovery of the β-glucosidase from the hydrogels were performed using 50 mM pH 5.0 citrate buffer. β-glucosidase activities and protein contents were measured in every step and applied to SDS-PAGE.

3. Results and Discussions

3.1 β-glucosidase imprinted hydrogel

The polyacrylamide matrix is non-charged and multiple weak interactions, like hydrogen bonds and dipole-dipole interactions are assumed to be responsible for the polymer-template interactions (Tong et al. 2001). Proteins are very complex and possess many potential recognition sites at their surface, such as charged amino acids and hydrophobic/hydrophilic regions (Verheyen et al. 2011). The polymerization of monomers in the vicinity of a template protein leads to the formation of a cavity with the shape and size of the imprinted template, and with the sites of interaction in a pre-determined orientation (Hjerten et al. 1997, Ghasemzadeh et al. 2008). It is well known that the diffusivity of proteins in a highly crosslinked polymer matrix is rather slow. Polymer geometry, polymer hydration, crosslink density, protein size and temperature all play a role in the time needed for a protein to diffuse into

the polymer matrix and to reach equilibrium (Verheyen et al. 2011).

β-Glucosidase from almonds is a homodimer consisting of 2 equal subunits of 65 kDa and is a glycoprotein. It has an isoelectric value of 7.3 and 6.7 nm molecular diameter (Grover et al. 1977, Gómez et al. 2012). Hydrogen bonding is the dominant driving force for the molecular recognition between β-glucosidase and the monomers (Fig. 1). Multiple-point hydrogen bonds could be produced when the cavities in the hydrogel had complementary interaction surface with the protein (Pan et al. 2009). Elution of β-glucosidase from polyacrylamide gel was performed using (pH 2.8). Negatively charged SDS micelles were interacted positively charged protein at this pH. Acetic acid could disrupt intramolecular hydrogen bonds within the protein molecule and so further helps to denature the protein (Hawkings et al. 2005)

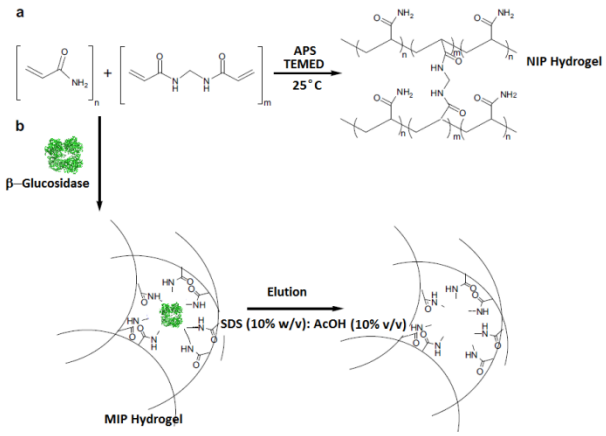

Figure 1. Proposed mechanism of a) NIP hydrogel b) β-glucosidase imprinted hydrogel (Adapted from Pan et al. 2009)

3.2 Characterization of the Imprinted and Non-imprinted Hydrogels

3.2.1 SEM Analysis

Scanning electron microscopy (SEM) has been an essential tool for characterizing the surface morphology and fundamental physical properties of the adsorbent. It is useful for determining the particle shape, porosity and appropriate size distribution of the adsorbent. As seen from Figure 2, unwashed MIP and NIP hydrogel have smooth and porous surface. To remove the template protein, MIP hydrogel was washed with SDS:AcOH 10% (w/v):10% (v/v) and then the surface of MIP hydrogel became rough and more porous.

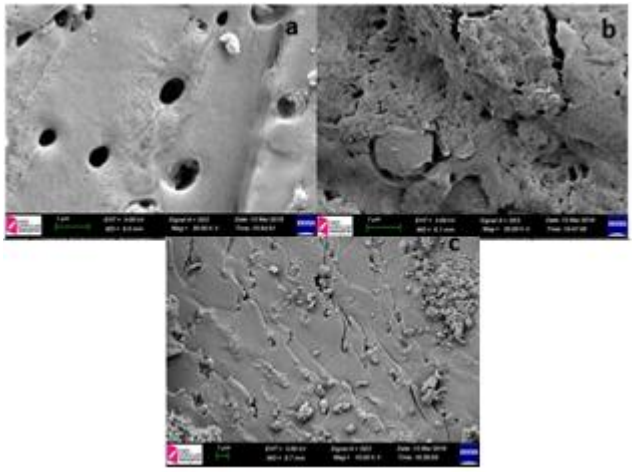

Figure 2. SEM micrographs of a) Unwashed MIP hydrogel (30000x) b) Washed MIP hydrogel (30000x) c) NIP hydrogel (10000x)

3.3 Optimization of Rebinding Conditions

3.2.1 Effect of contact time

The contact time between the enzyme and the hydrogel is an important parameter in enzyme separation by adsorption. 2.5 mg/mL β-glucosidase in phosphate buffer (0.1 M pH 7.0) was added to 0.01 g of hydrogel and incubated for determined time intervals. Fig. 3 shows the relationship between the adsorption capacity of MIP hydrogel (NIP) and the adsorption time. At room temperature, within the first 15 min the adsorption capacity increases rapidly. The rebinding reaches a plateau after about 120 min, indicating that the imprinted sites are saturated with β-glucosidase. The adsorption capacity of NIP hydrogel is much smaller than that of the MIP hydrogel. MIP hydrogels have adsorption cavities which are complementary to the template molecule in shape. Comparing this MIP with the NIP hydrogel, it is clear that a much higher rebinding capacity is achieved.

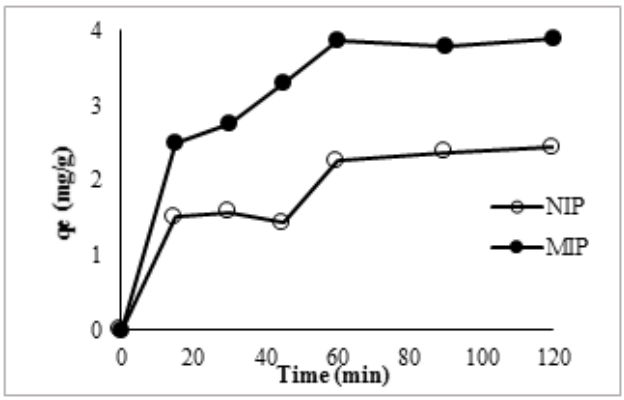

Figure 3. Effect of contact time on rebinding of β-glucosidase on MIP and NIP hydrogels.

3.3.2 Effect of pH

In this study, series of 2.5 mg/mL β-glucosidase solution were prepared in different pH values (0.1 M pH 3.0-4.0 acetate buffer, 0.1 M pH 5.0-6.0 citrate buffer, 0.1 M pH 7.0 phosphate buffer, 0.1 M pH 8.0 Tris-HCl buffer) and added on the hydrogels. After incubation at 25°C for 120 minutes, the amount of protein adsorbed on MIP and NIP hydrogels were calculated. As seen from Figure 4, the imprinting efficiency reached the maximum when the pH was 7.0 because the pH value affected the β-glucosidase conformation and charge.

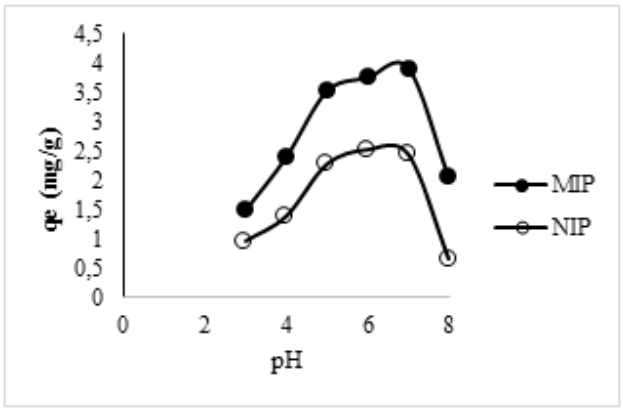

Figure 4. Effect of pH on rebinding of β-glucosidase on MIP and NIP hydrogels (contact time: 120 min, enzyme concentration 2.5 mg/mL).

3.3.3 Effect of temperature

In this study 2.5 mg/mL β-glucosidase solution (0.1 M pH 7.0 1 mL) was added to the hydrogels and shaken gently at various temperature values (25-40 °C) for 120 minutes. As seen from Figure 5, the adsorption of the enzyme β-glucosidase decreased with the increase in temperature. At 25°C it appears that MIP hydrogels have higher β-glucosidase selectivity than NIP hydrogels. β-glucosidase adsorption decreased with increasing temperature suggesting that the interactions between β-glucosidase and the hydrogel were based on hydrogen bonds.

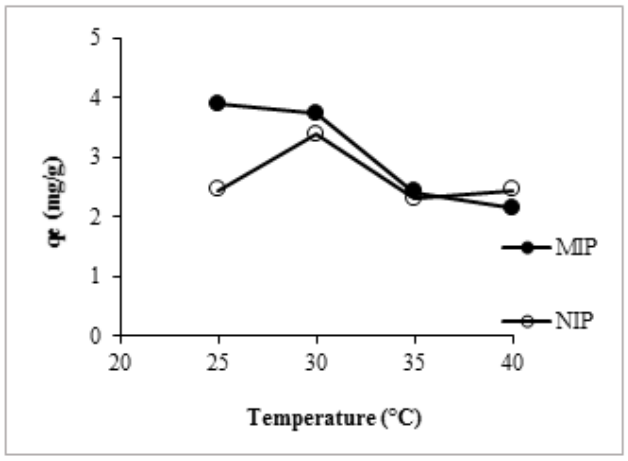

Figure 5. Effect of temperature on rebinding of β-glucosidase on MIP and NIP hydrogels (contact time: 120 min, enzyme concentration 2.5 mg/mL, pH 7.0).

3.3.4 Effect of initial β-glucosidase enzyme concentration

The adsorption isotherm experiments for MIP and NIP were carried out using different β-glucosidase concentrations in the range 1-3.5 mg/mL for 120 min accompanied by mild shaking. The other operational parameters (contact time, pH and temperature) were kept at optimum values. At low different β-glucosidase concentrations, was not enough to fill up the specific binding cavities (Fig. 6). The specific imprinted sites were gradually occupied and the adsorption capacity of MIP hydrogel became steady with increasing different β-glucosidase concentration, and the saturation value was achieved at β-glucosidase concentration of 3.5 mg/mL. The maximum adsorption capacities of MIP and NIP hydrogel were 3.74 and 2.53 mg/g, respectively and the IF value was calculated as 1.47. The results showed that MIP hydrogel had a higher adsorption capacity for β-glucosidase than that of NIP hydrogel.

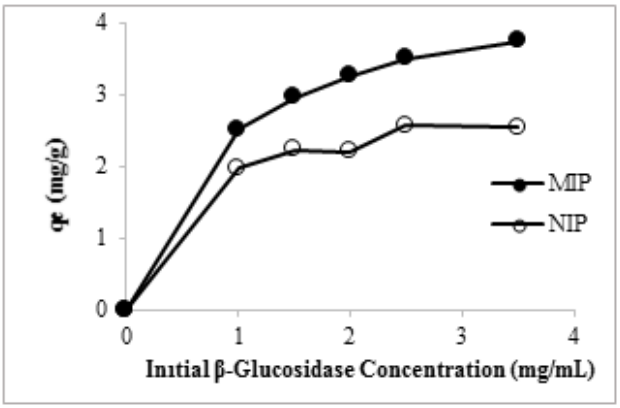

Figure 6. Effect of initial enzyme concentration on rebinding β-glucosidase on MIP and NIP hydrogels. (contact time: 120 min, temperature: 25 °C, pH 7.0).

3.4 Adsorption Isotherms

Equilibrium study is important as it provides the qualitative information on the nature of solute-solid surface interactions and could be used to evaluate the adsorption capacity of a particular adsorbent. In this study, two widely used isotherm models, i.e., Langmuir model and Freundlich model were used to describe the adsorption process. These isotherms are useful for estimating the total amount of adsorbent needed to adsorb a required amount of adsorbate from the solution.

Freundlich isotherm points a heterogeneous surface energy system and describes the adsorption process as ‘‘the ratio of the amount of solute adsorbed onto a given amount of adsorbent to the concentration of the solute in the solution is not constant at different concentrations’’. The logarithmic form of Freundlich model is given by the equation 5:

$$log\ qe = log\ Kf + \frac{1}{n} log\ Ce \quad (5)$$

where qe is the amount adsorbed and K_F and n are Freundlich constants related to the adsorption capacity and adsorption intensity, respectively. When log qe was plotted against log Ce, slope was obtained 1/n, were calculated from the slope and intercept of the plot log qe versus log Ce (shown in Fig. 7). K_F represents the amount of solute

adsorbed at an equilibrium concentration of unity and thus is a measure of the adsorption capacity of the material, while n reflects the adsorption intensity (Table 1).

Another widely used equation in adsorption processes is the Langmuir equation. Langmuir model is represented by the following equation 6:

$$\frac{Ce}{qe} = \frac{1}{Q^{\circ}b} + \frac{Ce}{Q^{\circ}} \qquad (6)$$

where Q^{o} is the amount of adsorbate at complete monolayer coverage (mg/g), which gives the maximum sorption capacity of sorbent and b (mL/mg) is the Langmuir isotherm constant that relates to the energy of adsorption calculated from the slope and intercept of the plot Ce/qe vs. Ce (shown in Fig. 8). The Langmuir constants Q^{o} and b are calculated and the values of these constants are tabulated for the highest R^2 value in the Table 1.

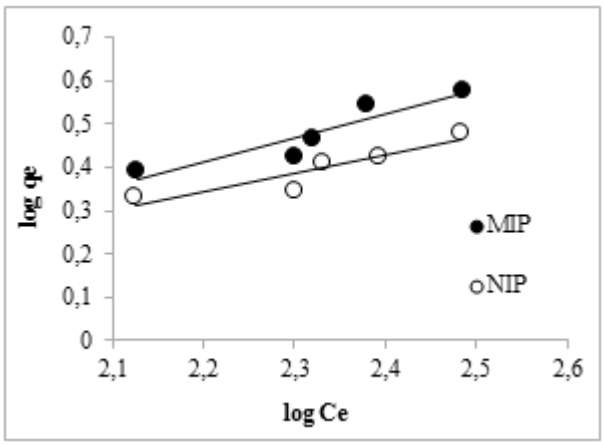

Figure 7. Freundlich isotherm graph of the adsorption assay of β-glucosidase on MIP and NIP hydrogels.

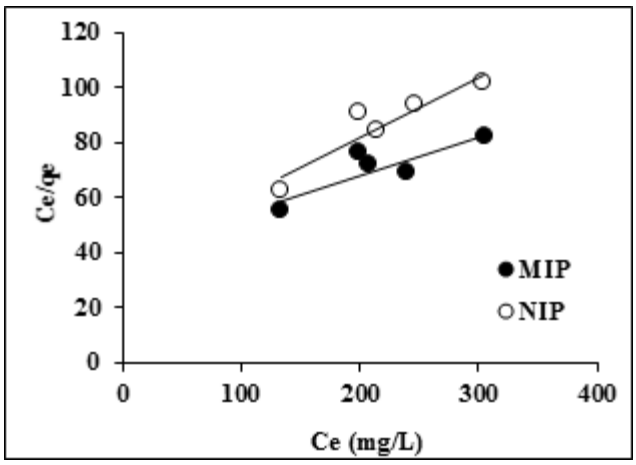

Figure 8. Langmuir isotherm graph of the adsorption assay of β-glucosidase on MIP and NIP hydrogels.

When R^2 values of adsorption models were compared, the adsorption of β-glucosidase on MIP and NIP hydrogels was fitted to the Freundlich equation (R^2 >0.87) and Langmuir equation (R^2 >0.86) respectively. This result demonstrates that the adsorption of β-glucosidase on MIP hydrogel can be characterized by multi-site adsorption isotherm. However adsorption of β-glucosidase on NIP hydrogel can better fit to Langmuir isotherm model suggesting that this adsorption is better to be described as a monolayer adsorption.

Table 1. Langmuir and Freundlich isotherm constants for adsorption of β-glucosidase on MIP and NIP hydrogels

Langmuir Isotherms		**Freundlich Isotherms**	
MIP	**NIP**	**MIP**	**NIP**
$\mathbf{Q_{max}}$= 7.2 mg/g	$\mathbf{Q_{max}}$=4.6 mg/g	$\mathbf{K_F}$=0.16 mg/g	$\mathbf{K_F}$=0.26 mg/g
b=0.0034 L/mg	**b**=0.0056 L/mg	**1/n**=0.55	**1/n**=0.42
$\mathbf{R_L}$= 0.105	$\mathbf{R_L}$= 0.066		
$\mathbf{R^2}$=0.733	$\mathbf{R^2}$=0.864	$\mathbf{R^2}$=0.879	$\mathbf{R^2}$=0.835

Dimensionless separation factor R_L is a used to analyze the adsorption process. When R_L value is between 0 and 1 or higher than 1, this means the adsorption process is favorable or unfavorable respectively. If R_L equals to 1 or 0 , it shows the adsorption process linear or irreversible respectively. [35] $R_{L,}$ can be expressed as:

$$R_L = 1/(1+bCo) \qquad (7)$$

Where b is the Langmuir constant and C_O is the initial β-glucosidase concentration (mg L^{-1}). Calculated R_L values for the adsorption of the enzyme onto MIP and NIP hydrogels were 0.105 and 0.066 respectively, showing that the adsorption process was favorable.

3.5 Kinetic parameters

Adsorption kinetics has an inseparable relationship with adsorption efficiency. The adsorption kinetic was investigated to measure the required equilibrium time for adsorption of β-glucosidase onto imprinted hydrogel. The adsorption kinetics of 2.5 mg/mL β-glucosidase solution at pH 7.0 was examined as a function of imprinted and non-imprinted hydrogels. In order to study the adsorption mechanism and verify the rate-determining step, pseudo-first-order and pseudo-second-order were utilized to fit the adsorption kinetics data. The nonlinear form of the mentioned two model equations can be expressed by equation (7) and (8), respectively:

$$log\ (qe - qt) = \log qe - \frac{k_1}{2.303} t \qquad (7)$$

qe and qt indicate the amount of protein adsorbed at equilibrium and at a specific time (mg/g) and k_1 (min^{-1}) is the first-order rate constant. First-order rate constant k_1 was

calculated from the slope value of the linear plot of log (qe-qt) vs. t (Figure 9).

$$\frac{t}{qt} = \frac{1}{k_2 qe^2} + \frac{t}{qt} \qquad (8)$$

where qe (mg/g) is the amount of protein adsorbed at equilibrium, qt (mg/g) is the amount of protein on hydrogels at time. t and k_2 [g/(mg min)] is the rate constant of pseudo-second-order adsorption. The values of $1/(k_2qe)^2$ and 1/qe are derived experimentally from the intercept and slope of the linear plots of t/qt versus t, which eventually leads to values of k_2 and qe (Fig. 10). Relationship existing between experimental data and pseudo-second-order model and the correlation coefficient (R^2) in Table 2 suggest a strong relationship between the parameters and also explain that the adsorption process of enzyme both followed pseudo-second-order kinetics. The theoretical q_e values were very well correlated with the experimental data in the case of pseudo-second-order kinetics. This also indicates that the adsorption process of the enzyme is controlled by chemisorption due to the several interactions between the enzyme and the functional groups of MIP and NIP hydrogels.

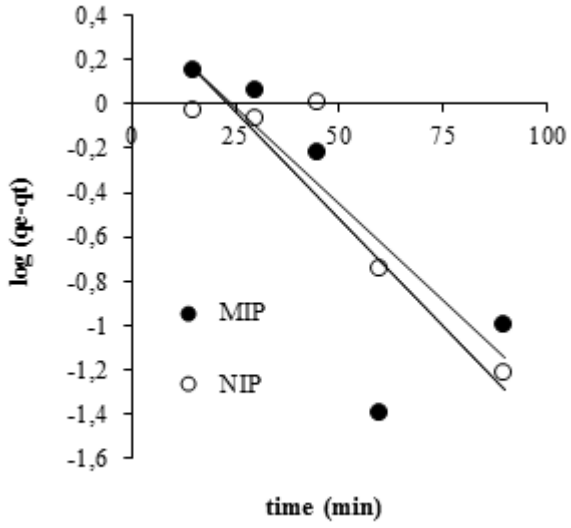

Figure 9. Pseudo-first-order model of the adsorption assay of β-glucosidase on MIP and NIP hydrogels.

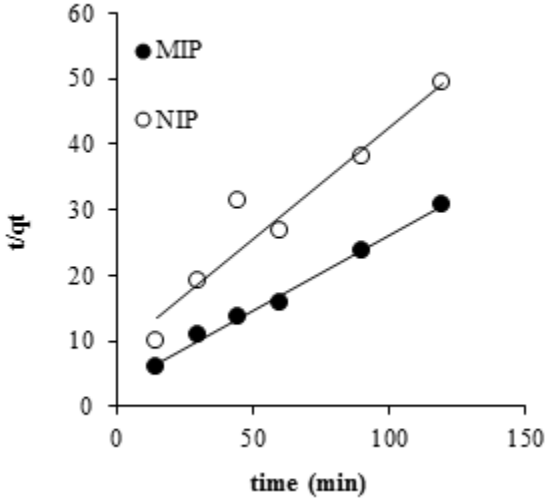

Figure 10. Pseudo-second-order model of the adsorption assay of β-glucosidase on MIP and NIP hydrogels.

Table 2. Kinetic Models

Pseudo-first-order model		Pseudo-second-order model	
MIP	**NIP**	**MIP**	**NIP**
$\mathbf{R^2}$=0.661	$\mathbf{R^2}$=0.840	$\mathbf{R^2}$=0.992	$\mathbf{R^2}$=0.920
$\mathbf{q_e}$ = 2.76 mg/g	$\mathbf{q_e}$ = 2.63 mg/g	$\mathbf{q_e}$= 4.36 mg/g	$\mathbf{q_e}$= 2.94 mg/g
$\mathbf{k_1}$ = 0.0437 min^{-1}	$\mathbf{k_1}$ = 0.0392 min^{-1}	$\mathbf{k_2}$= 0.0175 g/mg.min.	$\mathbf{k_2}$= 0.0137 g/mg.min.

3.6 SDS-PAGE analysis

The SDS-PAGE analysis is shown in Figure 11. Lane i and h present the standard protein mixture and pure β-glucosidase. Dialysis fraction (e) was applied on MIP and NIP hydrogels and then desorption of the enzyme from hydrogels was done using 50 mM pH 5.0 citrate buffer. Desorption fractions of MIP and NIP hydrogels are seen in lane (b) and (a) respectively. Only the band of desorbed enzyme from MIP hydrogel could be easily seen. The SDS-PAGE analysis suggests that MIP hydrogel could specifically absorb β-glucosidase from the dialysis fraction. These results show that MIP hydrogels could be use as an affinity matrix in enzyme purification steps.

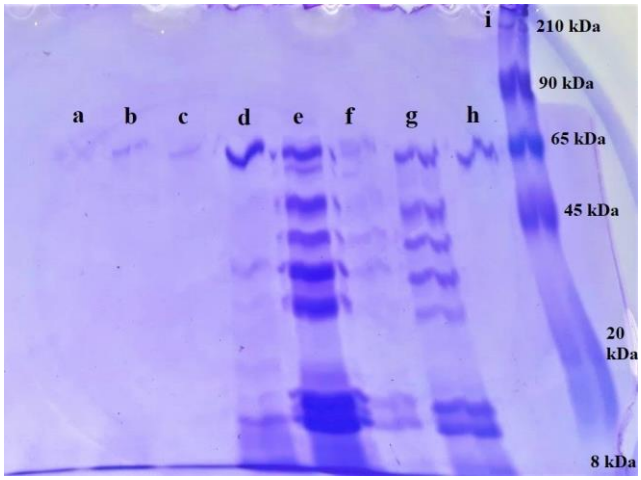

Figure 11 Results of SDS-PAGE analysis a) desorption of enzyme from NIP b) Desorption of enzyme from MIP c) unbound enzyme (MIP hydrogel) (10 fold dilution), d) unbound enzyme (MIP hydrogel) e) Dialysis fraction f) Acetone precipitation (5 fold dilution g) Acetone precipitation, h) Pure β-glucosidase i) protein molecular weight markers

4. Conclusions

β-Glucosidase imprinted hydrogel was successfully synthesized in the presence of monomer acrylamide and crosslinker N,N'methylenebisacrylamide. Proteins are very complex and possess many potential recognition sites at their surface, such as charged amino acids and hydrophobic/hydrophilic regions. Molecular size and shape memory effect are also the major factors affecting the imprinting formation and template recognition. The imprinted hydrogel exhibits significant recognition property and selectivity to target β-glucosidase. The easy preparation, and high selectivity of β-glucosidase imprinted hydrogel exhibit its potential application in β-glucosidase separation.

Acknowledgment

This work is supported by Scientific Research Project Office of Manisa Celal Bayar University (BAP 2017-003)

References

Bhattacharyya R and Ray SK 2013. Kinetic and equilibrium modeling for adsorption of textile dyes in aqueous solutions by carboxymethyl cellulose/poly(acrylamide-co-hydroxyethyl methacrylate) semi-interpenetrating network hydrogel. Polym Eng Sci 53(11):2439–2453.

Çelik A, Dinçer A, Aydemir T 2016. Characterization of β-glucosidase immobilized on chitosan-multiwalled carbon nanotubes (MWCNTS) and their application on tea extracts for aroma enhancement. Int J Biol Macromol 89:406–414.

Ergöçen Gözde. Purification and characterization of β-glucosidase from apricot (*Prunus Armeniaca*) seeds. Çukurova University, Institute of Natural and Applied Sciences, Department of Chemistry, Adana, 2013, 45. (M.Sc.).

Ghasemzadeh N, Nyberg F, Hjerten S 2008. Highly selective artificial gel antibodies for detection and quantification of biomarkers in clinical samples. I. Spectrophotometric approach to design the calibration curve for the quantification. J Sep Sci 31(22):3945-3953.

Gómez JM, Romero MD, Fernández TM, Díez E 2012. Immobilization of β-glucosidase in fixed bed reactor and evaluation of the enzymatic activity. Bioprocess Biosyst Eng 35:1399–1405.

Grover AK, Macmurchie DD, Cushley RJ 1977. Studies on almond emulsin beta-D-glucosidase. I. Isolation and characterization of a bifunctional isozyme. Biochim Biophys Acta. 482(1):98-108.

Hawkins DM, Derek S, Subrayal MR 2005. Investigation of protein imprinting in hydrogel-based molecularly imprinted polymers (HydroMIPs) Anal Chim Acta 542:61–65.

Hjerten S, Liao JL, Nakazato K, Wang Y, Zamaratskaia G, Zhang HX 1997. Gels mimicking antibodies in their selective recognition of proteins. Chromatographia 44(5-6):227-234.

Kempe M, Mosbach K 1994. Direct resolution of naproxen on a non-covalently molecularly imprinted chiral stationary phase J Chromatogr A 664 (2):276‑279.

Kimhi O, Bianco-Peled H 2007. Study of the interactions between protein-imprinted hydrogels and their templates, Langmuir 23, 6329-6335.

Li Z, Day M, Ding J, Faid K 2005. Synthesis and Characterization of functional methacrylate copolymers and their application in molecular imprinting. Macromolecules 38: 2620-2625.

Lv Y, Tan T, Svec F 2013. Molecular imprinting of proteins in polymers attached to the surface of nanomaterials for selective recognition of biomacromolecules, Biotechnol Adv 31:1172–1186.

Nishino H, Huang CS, Shea KJ 2006. Selective protein capture by epitope imprinting. Angew Chem 118:2452 –2456.

Pan J, Xue X , Wang J, Xie H, Wua Z 2009. Recognition property and preparation of Staphylococcus aureus protein A-imprinted polyacrylamide polymers by inverse-phase suspension and bulk polymerization. Polymer 50:2365–2372.

Pisarev OA, Polyakova IV 2018. Molecularly imprinted polymers based on methacrylic acid and ethyleneglycol dimethacrylate for L-lysine recognition. React Funcnt Polym 130:98-110.

Tong D, Heényi C, Bikádi Z, Gao J, Hjertén S 2001. Some studies of the chromatographic properties of gels ('Artificial antibodies/receptors') for selective adsorption of proteins. Chromatographia 54(1):7-14.

Verheyen E, Schillemans JP, Wijk M, Demeniex MA, Hennink WE, Nostrum CF 2011. Challenges for the effective molecular imprinting of proteins, Biomaterials 32:3008-3020

Verma OP, Singh A, Singh N, Chaudhary O 2011. Isolation, purification and characterization of β-glucosidase from *Rauvolfia serpentina*. J Chem Eng Process Technol 2:5.

Wanga DD, Gao D, Xu WJ, Li F, Yin MN, Fu QF, Xi ZN 2018. Magnetic molecularly imprinted polymer for the selective extraction of hesperetin from the dried pericarp of Citrus reticulata Blanco. Talanta 187:307-315.

Zaidi SA 2018. Development of molecular imprinted polymers based strategies for the determination of Dopamine. Sensor Actuat B Chem 265:488-497.

Zhao K, Chen T , Lin B, Cui W , Kan B , Yang N, Zhou X, Zhang X, Wei J 2015. Adsorption and recognition of protein molecular imprinted calcium alginate/polyacrylamide hydrogel film with good regeneration performance and high toughness. React Funcnt Polym 87:7–14.

Zhao M, Chen X, Zhang H, Yan H, Zhang H 2014. Well-defined hydrophilic molecularly imprinted polymer microspheres for efficient molecular recognition in real biological samples by facile RAFT coupling chemistry. Biomacromolecules 15(5):1663-75.

Eurasian J. Bio. Chem. Sci. 2(1): 24-28

EJBCS

Eurasian Journal of Biological and Chemical Sciences

Journal homepage: www.dergipark.org.tr/ejbcs

Alternanthera reineckii Briq.'nin doku kültürü çalışmaları için yüzey sterilizasyonunun optimizasyonu

Kübra Uğur, Muhammet Doğan*, Abdullah Kaya

Karamanoğlu Mehmetbey Üniversitesi, Kamil Özdağ Fen Fakültesi, Biyoloji Bölümü, Karaman, Turkey

*Corresponding author : muhammetdogan01@gmail.com
Orcid No: 0000-0003-3138-5903

Received : 10/05/2019
Accepted : 02/07/2019

Özet: Yüzey sterlizasyonu doku kültürü çalışmalarında ilk aşamadır. Bu aşamadan geçtikten sonra bitkilerin çoklu üretimleri mümkün olabilmektedir. Mevcut çalışma, *Alternanthera reineckii* Briq.'nin doku kültürü ile üretimi için yüzey sterilizasyonu çalışmalarını sunmaktadır. Ön sterilizasyon işlemi için *A. reineckii* 20 dk boyunca akan çeşme suyunun altında bekletilmiştir. Yüzey sterilizasyonu için üst gövdeden 3-5 cm uzunluklarında kesilen parçalar farklı süre (15 ve 30 dk) ve konsantrasyonlarda (%10-30) hidrojen peroksit (H_2O_2) ile muamele edilmiştir. Boğum eksplantları izole edilerek bitki büyüme düzenleyici içermeyen Murashige ve Skoog (1962) besin ortamına aktarılmıştır. Kültür ortamlarda ilk kontaminasyonlar 6. günde gözlenmeye başlamıştır. Kültür ortamlarında daha çok bakteriyel kontaminasyonlar gözlenmiştir. Yüksek H_2O_2 maruziyetinde eksplantların rejenerasyon kapasiteleri oldukça düşmüştür. Bazı eksplantlarda beyazlaşma ve sararmalar tespit edilmiştir. Hidrojen peroksit ile muamele edilen eksplantlarda bulaşık oranları %20-100 arasında değişmiştir. Steril ve canlı eksplant değerleri kullanılan H_2O_2 ile farklılık göstermiştir. En yüksek steril ve sağlam eksplantlar (%60) %25'lik H_2O_2 ile 15 dk uygulanan eksplantlarda, ardından ise (%55) %15'lik H_2O_2 ile 30 dk uygulanan eksplantlarda tespit edilmiştir. Buradan elde edilen steril ve canlı eksplantlar bitki büyüme düzenleyici içermeyen ortamlarında aktarılmış ve çoğaltım çalışmaları için stoklar oluşturulmuştur. Bu çalışma, *A. reineckii*'nin *in vitro* üretimi için gerekli sterilizasyon işlemleri için araştırmacılara yardımcı olabilir.

Anahtar Kelimeler: Boğum eksplantı, çoğaltım, H_2O_2, rejenerasyon, sterilizasyon

Optimization of surface sterilization of Alternanthera reineckii for tissue culture studies

Abstract: Surface sterilization is the first stage in tissue culture studies. After this stage, multiple productions of plants can possible. The present study presents surface sterilization studies for the production of *Alternanthera reineckii* Briq. by tissue culture. For the pre-sterilization process, *A. reineckii* was kept under the tap water flowing for 20 min. For surface sterilization, the parts cut at length 3-5 cm from the upper body were treated with hydrogen peroxide (H_2O_2) at different time (15 and 30 min) and concentrations (10-30%). The nodal explants were isolated and transferred to the nutrient medium of Murashige and Skoog (1962) which did not contain a plant growth regulator. The first contamination in the culture environment began to be observed on the 6th day. More bacterial contamination was observed in culture media. The regeneration capacity of the explants in highly H_2O_2 exposure decreased considerably. Whitening and yellowing were detected in some explants. Contamination rates in the explants treated with H_2O_2 ranged from 20 to 100%. The values of sterile and live explants were different with H_2O_2. The highest sterile and live explants (60%) were detected in explants with 25% H_2O_2 for 15 min followed by explants (30%) with 15% H_2O_2 for 30 min. The sterile and live explants obtained from this were transferred in non-plant growth media and stocked for propagation studies. This study may help researchers for the sterilization procedures required for *in vitro* production of *A. reineckii*.

Keywords: Nodal explant, propagation, H_2O_2, regeneration, sterilization

1. Giriş

Doku ve hücre kültürü çalışmalarında bitki doku ve organları, aseptik ve kontrollü şartlarda yetiştirilir. Bu teknik, temel olarak bitki hücrelerinin totipotensi özelliğine dayanır. Totipotensi, tek bir hücrenin, hücre bölünmesiyle tam genomu oluşturma yeteneğini ifade eder. Bitki hücresinin totipotent potansiyeli ile birlikte hücrelerin metabolizmalarını, büyümelerini ve gelişimlerini değiştirme kapasiteleri de aynı derecede

önemlidir (Rani ve Kumar, 2017). Bitki doku kültürü ortamı, bitkilerin normal büyümesi ve gelişimi için gerekli tüm besin maddelerini içerir. Esas olarak makro besinler, mikro besinler, vitaminler, diğer organik bileşenler, bitki büyüme düzenleyicileri, karbon kaynağı ve katı ortam durumunda bazı jelleştirici maddelerden oluşur. Murashige ve Skoog besiyeri (MS besiyeri), birçok bitki türünün *in vitro* vejetatif üremesi için yaygın şekilde kullanılır. Ortamın pH'ı, hem bitki büyümesini hem de bitki büyüme düzenleyicilerinin aktivitesini etkileyen önemli bir faktördür. Ortamın pH'ı 5.4 - 5.8 arasındaki değere ayarlanır. Kültür için hem katı hem de sıvı ortam kullanılabilir (Hussain ve ark., 2012; Bridgen ve ark., 2018).

Mikroorganizmalar doku kültürü çalışmalarında bulaşık/kontaminasyon olarak kabul edilir. *İn vitro* ortamlardaki bitki kültüründe en önemli kayıplar kontaminasyon yüzünden oluşur. Bu tür kontaminasyonlara; virüs, bakteri, maya, mantar vb. mikroorganizmalar sayılabilir (Oyebanji ve ark., 2009). Yapılan sterilazasyon yetersiz ise mantar, maya ve bakteri oluşabilir. Bitkiden aldığımız eksplant parçasında toprağa maruz kalan bitki parçalarını, tarlada, tropik iklimlerde yetişen bitkiler ile sucul bitkileri sterilize etmek genellikle zordur (Leifert, 2009).

Bitki doku ve hücre kültüründe kullanılan ortamlar, çeşitli besin maddeleri, mineraller, bitki yetiştirme maddeleri, vitaminler ve şeker kombinasyonlarını içerir. Ne yazık ki, bu kültür ortamı ayrıca bakteri ve mantarların hızlı büyümesi için de uygundur. Bu kontaminasyonlar, bitki dokusunu veya hücre kültürünü istila ettikleri için hızlı bir şekilde büyürler ve besin ortamını tüketir ve kültürlenmiş bitki dokusunun büyümesini etkiler ve nihayetinde öldürebilecekleri toksinler üretebilirler. Bu nedenle, tüm *in vitro* bitki kültürü manipülasyonları için steril tekniklerin kullanılması zorunludur. Doku kültürü sisteminin hazırlanması ve korunması, kültür ortamının sterilizasyonunu, kültürlenecek tohum veya bitki dokusunun yüzey sterilizasyonunu ve kullanılan herhangi alet ve ekipmanların sterilizasyonunu gereklidir. Bitki dokusunun manipülasyonu çalışmaları tipik olarak steril bir odada veya laminer hava akış kabini gibi kabinlerde gerçekleştirilmelidir. Bakteriler ve mantarlar ile kontaminasyon, bitki doku kültürlerini sürekli olarak tehdit eden sık görülen bir sorundur (Misra ve Misra, 2012).
Bu çalışma, sucul bir bitki olan *Alternanthera reineckii* Briq.'nin farklı derişimlerde ve sürede hidrojen peroksit ile yüzey sterilizasyonunu sunmaktadır.

2. Materyal ve Metot

Bitki materyali olarak kullanılan *A. reineckii*, İstanbul (Türkiye)'da bulunan akvaryumculardan temin edilmiştir. Yüzey sterilizasyonu işlemi uygulanmadan önce *A. reineckii*, 20 dk akan çeşme suyunun altında bekletilmiştir. Hidrojen peroksit uygulamasında (%35 H_2O_2 - Merck) *A. reineckii*, yüzey sterilizasyonu için üst gövdeden 3-5 cm uzunluklarında kesilen parçalar farklı süre (15 ve 30 dk) ve konsantrasyonlarda (%10-30) H_2O_2 ile muamele edilmiştir. 5 dk süreyle 3 kez durulama işlemi uygulandıktan sonra boğum eksplantları izole edilerek, hormonsuz Murashige ve Skoog (1962) (MS) besin ortamına aktarılmış ve bulaşık oranları belirlenmiştir.
Kültür ortamlarının hazırlanmasında MS besin tuzları ve %3 sükroz (Duchefa) kullanılmış ve jelleştirme ajanı olarak %0,65'lik agar (Duchefa) ilave edilmiştir. 1N NaOH ve 1N HCl ile kültür ortamının pH'sı 5.7±0.1'e yapılmış ve otoklavda steril edilmiştir (1.2 basınç - 120 ºC'de 20 dk). Denemelerde eksplantlar, beyaz ışık yayan diyotlar (LED) 24±1ºC'de ve 16 saat ışık fotoperiyodunda kültüre alınmıştır.

3. Bulgular ve Tartışma

Bitki doku kültüründe bakteriyel ve fungal kontaminasyonlar büyük bir tehdittir. Bitkiler dış kaynaklı olarak bakteri ve fungus barındırabilir. Bu dış kaynaklı kontaminasyonların uzaklaştırılması, doku kültürü çalışmalarının ilk ve en önemli aşamalarından biridir.
Bu çalışma, A. reineckii'nin yüzey sterilizasyonu için farklı süre ve konsantrasyonlarda H_2O_2 uygulamasını içermektedir. (Tablo 1). Daha sonra 5'er dk süre ile 3 defa durulama işlemi yapılmıştır. Bu durulama işlemleri H_2O_2'in zararını azaltmak için oldukça önemlidir. Bu üst gövde parçalarından izole edilen boğum eksplantları bitki büyüme düzenleyici içermeyen MS besin ortamına aktarılmıştır. Kültür ortamlarına yerleştirilen bu eksplantlarda kontaminasyonlar ortalama 6. günde gözlenmeye başlamıştır. Besin ortamlarında daha çok bakteriyel kontaminasyonlar gözlenmiştir (Şekil 1a). Fungal kontaminasyonlar az görülmekle beraber, genellikle 9. günden sonra daha belirgin olarak tespit edilmiş ve üç hafta sonunda yoğun olarak tüm ortam yüzeyini sarmıştır (Şekil 1b). Yüksek H_2O_2 etkisi ile eksplantlarda yüzey sterilizasyon başarılmış olsa da bu eksplantların rejenerasyon kapasiteleri oldukça düşmüştür. Genellikle H_2O_2 etkisi ile eksplantlarda beyazlaşma ve sararmalar tespit edilmiştir (Şekil 1c). H_2O_2 yüzey sterilizasyonu çalışmalarında oldukça tercih edilmektedir. Benzer şekilde, *Stevia rebundiana* Bertoni (Halim ve ark., 2016), *Colocasia esculenta* (Akshatha ve ark.,2018), *Prunus armeniaca* (Ozdemir ve Gur, 2018), *Rotala rotundifolia* (Buch-Ham. ex Roxb) Koehne (Dogan, 2017, 2019), bitkilerinin *in vitro* çoğaltımı için H_2O_2 kullanılmıştır.

Tablo 1. Farklı konsantrasyonlarda H_2O_2 ile muamale edilen *A. reineckii*'nin boğum eksplanlarının yüzey sterilizasyonu verileri

Hidrojen Peroksit (H_2O_2)		**Bulaşık Oranı (%)**	**Steril ve Ölen Eksplant Oranı (%)**	**Steril ve Canlı Eksplant Oranı (%)**
%	**Süre (dk)**			
10	15	100	-	-
15	15	100	-	-
20	15	70	10	20
25	15	30	10	60
30	15	30	25	50
10	30	40	20	40
15	30	25	30	55
30	30	20	80	-

Chalenko ve Cherednıchenko (2017) *A. reineckii*'nin yüzey sterilizasyonu için üç farklı dezentektan kullanmıştır. Bitki parçalarını % 0.1 civa (II) klorür çözeltisi (1, 2 ve 3 dk), % 10 H_2O_2 çözeltisi (1, 2 ve 3 dk), %5 sodyum hipoklorit çözeltisi (1, 2 ve 3 dk) bekleterek yüzey sterilizasyonunu başarmıştır. Bir diğer dezenfektan olan çamaşır suyu (NaCIO) da birçok sucul bitkinin yüzey sterilizasyonu için kullanılmıştır (Dogan 2018a, 2018b).

Kültür ortamında steril olan sürgünlerin bulunduğu bazı ortamlarda yaklaşık bir ay sonra bakteriyel kontaminasyonların çıktığı gözlenmiştir. Bu bakteriyel kontaminasyonlar bize eksplantların endojenik bakteri içerdiğini düşündürmüştür. Çünkü, bazı bitki türleri ile yapılan başarılı yüzey sterilizasyonu işlemlerinden sonra bile bakteriyel bulaşıkların çıktığı daha önce bildirilmiştir (Karaoğlu, 2010; Karaoğlu ve ark., 2006). Bitkilerin kökleri yaprak ve gövdeleri ile sürekli dış çevre ile etkileşim halindedir. Bu etkileşimler ile bazı bakteri türleri bitkilerin iç dokularında yaşayabilir veya bulanabilirler (Ryan ve ark., 2008; Sülü ve ark., 2016). Sterilizasyon denemeleri ikinci haftanın sonunda tamamlanmış ve bulaşık oranları (%), steril ve ölen eksplant oranı (%) ve steril ve sağlam eksplant oranı (%) verileri alınmıştır (Tablo 1).

Hidrojen peroksit ile muamele edilen eksplantlarda bulaşık oranları %20-100 arasında değişmiştir (Tablo 1). En yüksek bulaşık oranı (%100) %10 ve 15'lik H_2O_2 ile 15 dk muamele edilen eksplantlarda belirlenmiştir. Kullanılan H_2O_2 seviyesi ve süresi arttıkça ortamlardaki bulaşık yüzdesi düşüş göstermiştir. En düşük bulaşık yüzdesi (%20) %30'luk H_2O_2 ile 30 dk muamele edilen eksplantlarda gözlenmiştir. Ardından ise (%25) %15'lik H_2O_2 ile 25 dk muamele edilen eksplantlarda belirlenmiştir. Kullanılan H_2O_2 etkisi ile bazı eksplantlarda ölümler gözlenmiştir. Bunlar içerisinde steril olmasına rağmen ölen eksplantlar da tespit edilmiştir (Tablo 1). Steril ve ölen eksplant yüzdeleri %10-80 arasında değişmiştir. En yüksek steril ve ölü eksplant değeri (%80) %30'luk H_2O_2 ile 30 dk muamele edilen eksplantlarda belirlenmiştir. Bu karşın, %10 ve 15'lik H_2O_2 ile 15 dk uygulanan eksplantlarda herhangi bir ölü eksplant tespit edilmemiştir.

Steril ve canlı eksplant değerleri kullanılan H_2O_2 ile farklılık göstermiştir (Tablo 1). En yüksek steril ve sağlam eksplantlar (%60) %25'lik H_2O_2 ile 15 dk uygulanan eksplantlarda (Şekil 1d), ardından ise (%55) %15'lik H_2O_2 ile 30 dk uygulanan eksplantlarda kaydedilmiştir. Altı hafta sonunda steril ve sağlam eksplantlardan rejenere sürgünler elde edilmiştir (Şekil 1e). En düşük steril ve canlı eksplantlar ise (%20) %20'lik H_2O_2 ile 15 dk muamele edilen eksplantlarda tespit edilmiştir. Buradan elde edilen steril ve canlı eksplantlar bitki büyüme düzenleyici içermeyen ortamlarında aktarılmış ve çoğaltım çalışmaları için stoklar oluşturulmuştur. Dogan (2019) *R. rotundifolia*'nın yüzey sterilizasyonuna için ön işlem olarak 10 dk akan çeşme suyunda bekletilmiş ve ardından %20 oranında H_2O_2 ile 10 dk muamele ederek sterilizasyonu başarmıştır. Ghasheem ve ark. (2018) %5 ve 10'luk oranlarında H_2O_2 10 ve 20 dk süresince *Prunus persica* (L.) Batsch'nın sürgün ucu ve boğum eksplantlarının yüzey sterilizasyonu için denemeler kurmuştur. En yüksek steril ve sağlam eksplantları sürgün ucu için %10'luk H_2O_2 ile 20 dk muamelesi sonucu elde ederken (%25), boğum eksplatlarında %10'luk H_2O_2 ile 10 ve 20 dk muamelesi sonucu elde ettiğini (%20) bildirmiştir.

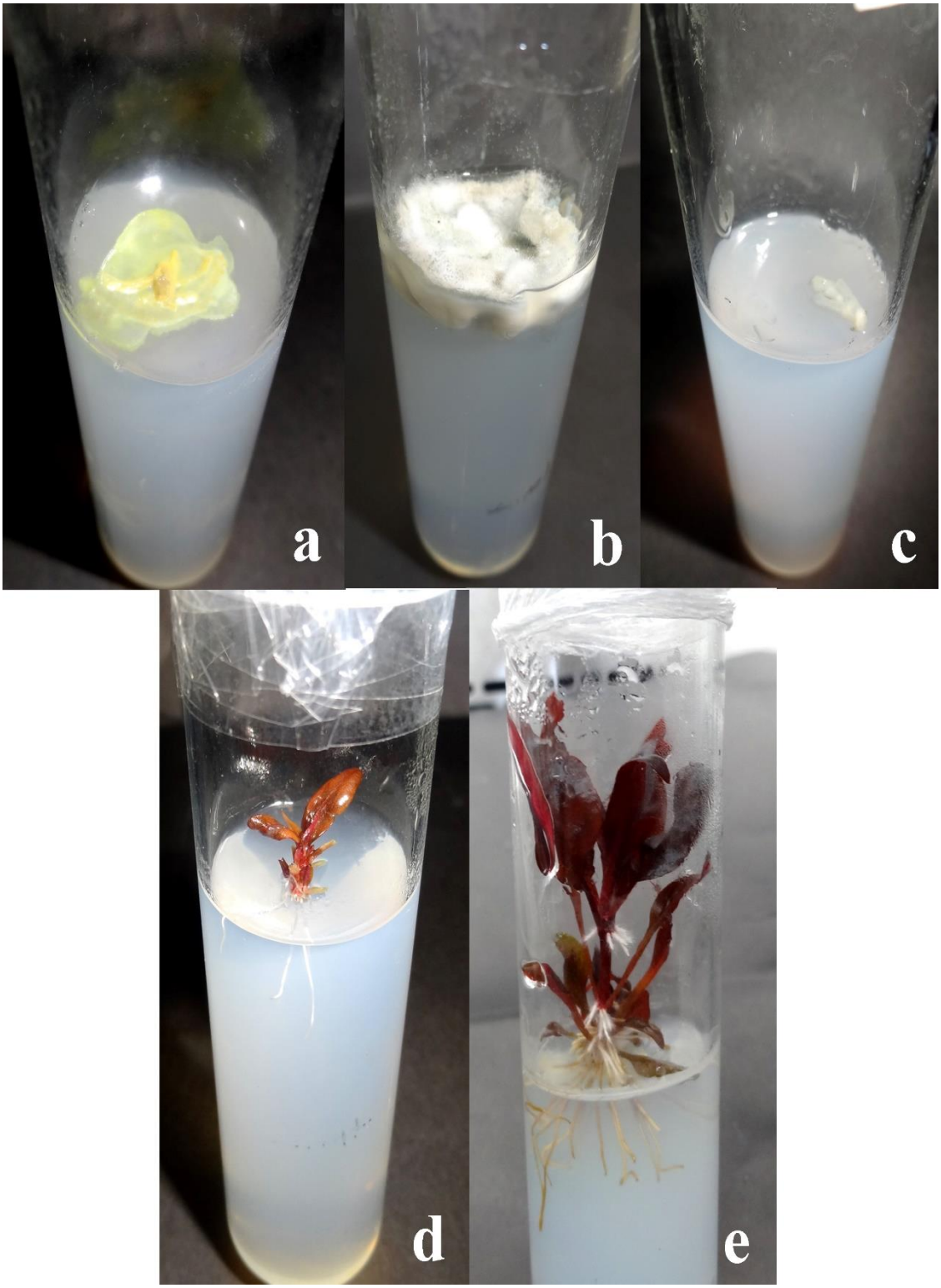

Şekil 1. Farklı konsantrasyonlarda ve sürelerde H_2O_2 uygulanan *A. reineckii* eksplantları. (a) eksplant üzerinde bakteriyel bulaşık (b) fungal bulaşık, (c) H_2O_2 etkisinden dolayı beyazlaşan eksplant (d) üç hafta sonunda %25'lik H_2O_2 ile 15 dk muamale edilen eksplanttan çıkan steril-sağlam sürgün (e) altı hafta sonunda büyüyen ve gelişen sürgün

Sonuç

Doku kültürü çalışmalarının en zor aşamlarından biri bitki yüzey sterilizasyonu işlemleridir. Çoğaltımda kullanılacak bitki parçaları steril edilmeden üretim aşamasına geçilememektedir. Bu çalışmada, önemli sucul bitki *A. reineckii*'nin yüzey sterilizasyonu H_2O_2 ile başarılı şekilde sağlanmıştır. Ortamlarda genel olarak bakteriyel kontaminasyonlar gözlenmiştir. En yüksek kontaminasyon

oranı (%100) %10 ve 15'lik H_2O_2 ile 15 dk muamele edilen eksplantlarda tespit edilmiştir. En fazla steril ve sağlam bitkiler %25'lik H_2O_2 ile 15 dk bekletilen eksplantlarda kaydedilmiştir. Bu rapor, *A. reineckii*'nin sterilizasyonu işlemleri ve doku kültürü çalışmaları için yardımcı olabilir.

Kaynaklar

Akshatha MD, Kavadikeri S, Rao NN 2018. *In vitro* micropropagation and antioxidant assay in *Colocasia esculenta*. Plant Tissue Cult Biotechnol 28(2):183-190.

Chalenko YV, Cherednichenko MY 2017. *In vitro* introduction and cultivation of aquatic plant *Alternanthera reineckii* Briq. The 3rd International Symposium on EuroAsian Biodiversity, 05-08 July 2017, Minsk - Belarus.

Bridgen MP, Van Houtven W, Eeckhaut T, 2018. Plant Tissue Culture Techniques for Breeding. In: Van Huylenbroeck J. (eds) Ornamental Crops. Handbook of Plant Breeding, vol 11. Springer, Cham

Dogan M 2017. Multiple shoot regeneration from shoot tip and nodal explants of *Rotala rotundifolia* (Buch-Ham. ex Roxb) Koehne. Ant J Bot 1(1,2): 4-8.

Dogan M 2018a. *In vitro* micropropagation from nodal explants of the medicinal plant *Lysimachia nummularia* L.. KSU J Agric Nat 21(6): 875-881.

Dogan M 2018b. *In vitro* shoot regeneration of *Limnophila aromatica* (lamk.) Merr. from nodal and internodal explants. Iğdır Univ. J. Inst. Sci. & Tech., 8(3): 77-84.

Dogan M 2019. Callus formation from full leaf and leaf parts of *Rotala rotundifolia* (Buch-Ham. ex Roxb) Koehne. Acta Biologica Turcica 32(2): 78-83.

Ghasheem AL, Stănică N, Petıcılă FAG, Venat O, 2018. *In vitro* effect of various sterilization techniques on peach (*Prunus persica* (L.) Batsch) explants. Scientific Papers, 227.

Halim MA, Alam MF, Rahman MH, Hossain MB, Uddin MB 2016. Sterilization process for *in vitro* regeneration of Stevia (*Stevia rebundiana* Bertoni). Int J Bus Soc Sci Res 4(4): 320-323.

Hussain A, Qarshi IA, Nazir H, Ullah I 2012. Plant Tissue Culture Current Status and Opportunities. In Recent advances in plant *in vitro* culture. IntechOpen.

Karaoğlu C 2010. Soğanlı bitkiler ve *in vitro* hızlı çoğaltım. Tarla Bitk Merk Araştırma Enstitüsü Derg 19 (1-2): 24-29.

Karaoğlu C, Çöçü S, İpek A, Parmaksız İ, Uranbey S, Sarıhan EO, Arslan N, Kaya MD, Sancak C, Özcan S, Gürbüz B, Mirici S, Er C, Khawar KM 2006. *In vitro* micropropagation of saffron. Proceedings of The 2nd International Symposium on Saffron Biology and Technology, Acta Horticulture, Number 739: 223-227.

Leifert C, Ritchie JY, Waites WM 1991. Contaminants of plant-tissue and cell cultures. World J Microbiol Biotechnol 7: 452-469.

Misra AN, Misra M, 2012. Sterilisation techniques in plant tissue culture. Life Science Center, Fakir Mohan University, Balasore-756020.

Murashige T, Skoog F 1962. A revised medium for rapid growth and bioassays with tobacco tissue cultures. Physiol Plant 15: 473-497.

Oyebanji OB, Nweke O, Odebunmi O, Galadima NB, Idris MS, Nnodi UN, Afolabi AS, Ogbadu GH 2009. Simple, effective and economical explant-surface sterilization protocol for cowpea, rice and sorghum seeds. Afr J Biotechnol 8(20): 5395-5399.

Ozdemir FA, Gur N 2018. *In vitro* propagation of cataloglu apricot (*Prunus armeniaca* L.) cultivar using apical node as explant. Prog Nutr 20(1-S) :176-181.

Rani A, Kumar S, 2017. Tissue culture as a plant production technique for medicinal plants: a review. International Conference on Innovative Research in Science, Technology and Management 6(1): 784-795.

Roberto T, Francesca M 2011. Sustainable sourcing of natural food ingredientsby plant cell cultures. Agro Food Industry Hi Tech, 22: 26-28.

Ryan RP, Germaine K, Franks A, Ryan DJ, Dowling DN 2008. Bacterial endophytes: recent developments and applications. FEMS Microbiol Letts 278: 1-9.

Sharma S, Rathi N, Kamal B, Pundir D, Kaur B, Arya S 2010. Conservation of biodiversity of highly important medicinal plants of India through tissue culture technology- a review. Agric Biol J N Am 1(5): 827-833.

Sülü SM, Bozkurt İA, Soylu S, 2016. Bitki büyüme düzenleyici ve biyolojik mücadele etmeni olarak bakteriyel endofitler. MKU Ziraat Fakültesi Derg 21(1): 103-111.

Eurasian J. Bio. Chem. Sci. 2(1): 29-37

EJBCS

Eurasian Journal of Biological and Chemical Sciences

Journal homepage: www.dergipark.org.tr/ejbcs

The effects of oral antidiabetics on adipogenesis related gene expressions in 3T3-L1, AML12 cell lines and their co-cultures

Meliha Koldemir Gündüz[1*], Mehtap Çevik[2], Penbe Çağatay[3], Belgin Süsleyici[2]

*[*1]Kütahya University of Health Sciences, Faculty of Engineering and Natural Sciences, Kütahya, Turkey*

[2]Marmara University, Faculty of Science and Arts, Department of Molecular Biology, Istanbul, Turkey

[3]Istanbul University, Faculty Medical, Department of Biostatistics and Medical Informatics, Istanbul, Turkey

*Corresponding author : *meliha.koldemirgunduz@ksbu.edu.tr*
Orcid No: 0000-0003-0969-6377

Received : 13/07/2019
Accepted : 20/07/2019

Abstract: The objective of the study was investigated for the effects of oral antidiabetic drugs, how they effect the cells proliferation activities and how they change the expressions of FTO, CD68, NIBAN, and RAN genes which could change insulin signalization and also be effective in the adipogenetic process on 3T3-L1 adipocytes, AML12 hepatocytes and adipocyte-hepatocyte co-cultures. Cell proliferation was examined real time with iCELLigence system and measured for 96 hours each 15 min period. The time and amount of active substances of the oral anti-diabetic drugs which were applied to cells were determined real time according to IC50 value. FTO, CD68 NIBAN and RAN gene expression profiles were determined with qPCR. When single and multiple doses of glipizide and acarbose in co-culture's were compared respectively, the 24 hour IC50 values were determined as 180 µM and 17 mg/ml in adipocytes; 72 µM and 23 mg/ml in hepatocytes, 41.5 µM and 5 mg/ml in coculture cells. The application of metformin for 24 hour IC50 value in single culture was determined as 175 mM in adipocytes and 2.3 mM in hepatocytes. In the Metformin administered cells. FTO, CD68 and NIBAN gene expressions were decreased in all groups. In the acarbose applied cells FTO and CD68 gene expressions were decreased in all groups. In the acarbose applied cells while NIBAN gene expression was decreased in adipocytes, it was fund to increase in co-cultured adipocytes. In the acarbose applied cells RAN gene expression was found to increase in all groups. Decreasing effects of antidiabetics on CD68 and FTO expressions may show protective effect of drug on inflammation and obesity. In conclusion, oral antidiabetic drug use may be effective in development glucose homeostasis via changing the gene expression of RAN in hepatocytes and adipocytes, this pathway may have therapeutic effect and provide novel strategies for treatment of insulin resistance.

Keywords: 3T3-L1 adipocyte, AML12 hepatocyte, iCELLigence system, oral antidiabetics, non-alcholic fatty liver disease, gene expression

1. Introduction

Obesity is a complex medical condition caused by excessive fat accumulation in the body caused by excessive consumption of foods and low levels of physical activity (Vasanth Rao et al., 2019). Obesity is a risk factor for type 2 diabetes mellitus (T2DM), hypertension, cardiovascular diseases, metabolic syndrome and cancer (Koldemir et al., 2012). Obesity not only contributes to other health problems, but also reduces quality of life and increases healthcare costs (Vasanth Rao et al., 2019). Type 2 diabetes mellitus (T2DM) is usually formed by the interaction of genetic and environmental factors and resulting in excessive increase in blood glucose levels, chronic, complex, and is a common metabolic disorder (Prokopenko et al., 2008). Type 2 diabetes, insulin secretion and activity of (fat, muscle and liver) is characterized by deterioration and associated with obesity (Prokopenko et al., 2008). The pathogenesis of type 2 diabetes beta cell dysfunction, insulin resistance and increase hepatic glucose takes place (Reaven, 1995). There are several genetic disorders that cause T2DM. This genetic disorder of glucose, lipid and protein metabolism leads to the formation of T2DM (Türkün, 2008). Obesity, hyperglycemia, hypertension, and plasma lipid abnormalities accompanied by insulin resistance (Reaven, 1995). Non-alcoholic fatty liver disease (NAFLD) affects 25% of the population and treatment options are limited (Niu et al., 2019). Non-alcoholic fatty liver disease (NAFLD) is closely associated with obesity, hypertriglyceridemia and diabetes. (Sanyal, 2003). NAFLD is a costly medical disease and continues to grow in parallel with the increasing prevalence of obesity and type 2 diabetes (Younossi et al., 2016). The liver and adipose tissue originate from a multipotent cell. Thus, the key molecules and signaling systems of adipose tissue and liver are regulated by common or overlapping metabolic and immune function pathways (Wellen and Hotamisligil, 2005; Shoelson et al., 2006).

Fat mass and obesity-associated gene (FTO) located on 16 q12.2 chromosome region is highly expressed in the hypothalamus and is suggested to play an important role in controlling energy homeostasis (Yuzbashian et al., 2019). In genome wide association studies, FTO gene polymorphisms were associated with increased risk obesity (Frayling et al., 2007; Dina et al., 2007; Scuteri et al., 2007). It has been reported that FTO gene over expression induced obesity (Rösen et al., 2001; Stratigopoulos et al., 2008). CD68 is a member of the lysosome associated membrane protein family that is restricted in its expression to cells of the monocyte/macrophage lineage. Weisberg et al. (2003) reported that up to 50% of the cells in the adipose tissue were positive for CD68. Reduction of inflammatory gene expression in adipose tissue has also been associated with weight loss in obese subjects (Clement et al., 2004; Cancello et al., 2005). The NIBAN gene, which is a member of the FAM129A gene family and consists of 14 exons, is located on the 13th chromosome in rats and the 1st in human and mice (Adachi et al., 2004). NIBAN regulates protein synthesis by modulating the phosphorylation of eukaryotic translation initiator factor 2α (eIF2α), p70 ribosomal S6 kinase 1 subunit and eukaryotic translation initiator factor 4E binding protein 1 (Sun et al., 2007). NIBAN plays a role in adipogenesis with unknown mechanism (Ye et al., 2011). RAN (LOC100045999 GTP-binding nuclear protein Ran) protein regulates a multitude of cellular responses, including nucleo-cytoplasmic shuttling, various aspects of mitosis, and other cytoplasmic transport mechanisms in specialized cell types (Segev, 2011; Clarke and Zhang, 2008; Yudin and Fainzilber 2009). Ran signaling is highly evolutionary conserved, and is thought to be essential for cellular homeostasis (Ye et al., 2011). RAN protein plays a role in adipogenesis with unknown mechanism (Ye et al., 2011).

There are many antidiabetic agents used in routine detavitation such as insulin, biguanides, sulfonylureas, thiazolidindiones (TZDs), sodium-glucose cotransporter type 2 inhibitors(SGLT2i), dipeptidyl peptidase 4 (DPP-4) inhibitors, glucagon-likepeptide 1 (GLP-1 receptor agonists) and α glucosidase inhibitors (AGis) (American Diabetes Association, 2018). Biguanides (especially metformin) are widely used for the treatment of T2DM and exhibit hypoglycemic effects by inducing insulin sensitivity and peripheral glucose uptake, reducing hepatic gluconeogenesis, reducing glucose reabsorption of the intestine (Yaribeygi et al., 2019). Sulfonylureas is a class of hypoglycemic antidiabetic drugs that increase insulin release from cells (Yaribeygi et al., 2019). Alpha glycosidase inhibitors inhibit the α-glycosidase enzymes in the small intestine and thus delay the absorption of carbohydrates (Yaribeygi et al., 2019).

In this study, the proliferative effect of AML12 hepatocytes, 3T3-L1 adipocyte and their co-culture by continuous monitoring assay was performed to investigate cytotoxicity of commonly used oral antidiabetic drug metformin, acarbose and glipizide and we sought to determine the effects of oral antidiabetic drug metformin on FTO, CD68, NIBAN and RAN gene expressions in AML12 hepatocytes, 3T3-L1 adipocyte and their co-culture.

2. Materials and Method

2.1.Cell Culture

Murine AML12 hepatocytes and 3T3-L1 fibroblasts were purchased from the American Type Culture Collection (ATCC) (Manassas, USA). 3T3-L1 cells were cultured in glucose-free Dulbecco's Modified Eagle's Medium (DMEM) supplemented with 10% fetal calf serum, penicillin (100 units/ml), and streptomycin (100 µg/ml) in a humidified atmosphere of 5% CO2 at 370C, with a change of medium every 2-3 days. AML12 cells and co-culture cells were cultured in a 1:1 mixture of Dulbecco's modified Eagle's medium and Ham's F12 medium with 0.005 mg/ml insulin, 0.005 mg/ml transferrin, 5 ng/ml selenium, and 40 ng/ml dexamethasone, 90%; fetal bovine serum, penicillin (100 units/ml), and streptomycin (100 µg/ml), 10% in a humidified atmosphere of 5% CO2 at 370C with a change of medium every 2-3 days. Sub-cultured as necessary by routine trypsinization method.

2.2.Differentiation of 3T3-L1 preadipocytes

3T3-L1 cell differentiation was based on the protocol by Miard et al. (2008). Cells were grown in DMEM medium until 80% confluency. Two days after confluency (Day 0), cells were washed with phosphate buffered saline (PBS) and fed with adipocyte differentiation media (DMEM, 10% fetal calf serum, 1 µM dexamethasone, 10 µg/mL insulin, and 0.25 mM 3-methyl-1-isobutylxanthine) for 2 days. Two days (Day 2) post induction, medium was supplemented with only 10 µg/mL insulin and replaced every 2 days until terminal differentiation.

2.3.Oil Red O Staining

Cells were washed with PBS and then fixed for 1 hour with 10% formalin solution. 60% isopropanol was added to each well and let sit for 5 minutes. Oil red O was diluted with water (3:2), filtered through a 0.22µm filter and incubated with the fixed cells for 5 min at room temperature. Cells were washed with water and the stained lipid droplets in the cells.

2.4.Cytotoxicity assay using iCELLigence system

The optimal cell concentration for proliferation experiments of AML12 hepatocytes, of 3T3-L1 adipocytes and their co-culture were determined. After seeding the cells in 150 µL medium to each well of the E-plate 8, the proliferation of cells were monitored every 15 min by the iCELLigence system. Approximately 24h after seeding, the AML12 cells were subjected to 50 µL of medium containing the following substances: acarbose (2.5 mg/ml, 5 mg/ml, 7.5 mg/ml, 10 mg/ml, 15 mg/ml, 25 mg/ml and

50 mg/ml), glipizide (100 µM, 150 µM and 500 µM) and metformin (0.5 mM, 1 mM, 2 mM, 4 mM, 5 mM, 7.5 mM and 10 mM). Approximately 24h after seeding, the 3T3-L1 cells were subjected to 50 µL of medium containing the following substances: acarbose (2.5 mg/ml, 5 mg/ml, 7.5 mg/ml, 10 mg/ml, 15 mg/ml, 25 mg/ml and 50 mg/ml), glipizide (100 µM, 250 µM and 500 µM) and metformin (5mM, 10mM, 25mM, 50mM, 100mM, 150mM and 250mM). Approximately 24h after seeding, the co-culture cells were subjected to 50 µL of medium containing the following substances: acarbose (1 mg/ml, 2 mg/ml, 4 mg/ml, 5 mg/ml, 7.5 mg/ml and 10 mg/ml), glipizide (100 µM, 150 µM and 500 µM) and metformin (10 mM, 25 mM, 50 mM, 75 mM and 100 mM). Only culture medium was added to control cell group. All experiments were monitored up to 96h.

2.5.RNA Isolation and Real-Time PCR Analysis

Total RNA was extracted from cells using the High Pure RNA Tissue Kit (Roche, Germany) according to the manufacturers instructions. Total RNA samples were diluted in DNase–RNase free sterile water and stored at −80°C until use. For cDNA synthesis, transcriptor HiFi cDNA synthesis kit was used (Roche, Germany). Expression of FTO, CD68, NIBAN and RAN genes were determined by quantitative real-time PCR using a LightCycler Nano (Roche Diagnostics, Germany) instrument. Measurements were carried out on at least three occasions for each sample. Cq values lower than 40 were not included to advanced statistival calculations. The expression amounts were calculated by using the reference gene (GAPDH) expression. Existence of specific gene products were confirmed with melting curve analysis. The gene expressions studies were repeated three times.

2.6.Statistical analysis

For the evaluation of results obtained from the iCELLigence system, statistical analyses were performed using the iCELLigence system software. The system software make a curve-fitting of elective "sigmoidal dose–response equation" to the experimental data points and calculates logarithmic half maximum inhibition concentration (log [IC50]) values. Results are presented as mean±SE. Statistical analysis was performed with SPSS software (version 16.0; SPSS Inc., Chicago, IL). In general, statistical differences between two groups were evaluated by the Wilcoxon signed ranks test and for comparison of multiple groups Friedman test (followed by Wilcoxon signed ranks test) was used. A p-value below 0.05 was considered significant.

3. Results

3.1.Effects of Antidiabetic Drugs over Proliferation of 3T3-L1 Adipocyte

To investigate the effect of oral antidiabetic drugs on proliferation, 3T3-L1 adipocytes were cultured for 24 h in standard medium (untreated). 100 µM, 250 µM and 500 µM glipizide were applied to the cell culture medium. While 500 uM glipizide had a lethal effect for adipocytes, 250 µM glipizide application has an antiproliferative effect on adipocytes. IC50 values were determined as 180 µM after 24h glipizide administration. The 3T3-L1 adipocytes were treated with 2.5, 5, 7.5, 10, 15, 25 and 50 mg / ml acarbose. The dose of acarbose applied to adipocyte cells did not have a lethal effect while producing cytotoxic effects on cells. IC50 values were determined as 17 mg/ml after 6h acarbose administration. 5, 10, 25, 50, 100, 150 and 250 mM metformin were applied to 3T3-L1 adipocyte cells. 5, 10, 25, 50 mM metformin administration had antiproliferative effect in 3T3-L1 adipocytes and 250 mM metformin had lethal effect for adipocytes. The IC50 value at 24 hours was calculated as 175 mM as a result of metformin administration.

3.2.Effects of Antidiabetic Drugs over Proliferation of AML12 Hepatocye

To investigate the effect of oral antidiabetic drugs on proliferation, AML12 hepatocytes were cultured for 24 h in standard medium (untreated). 100 µM, 250 µM and 500 µM glipizide were applied to the cell culture medium. 500 µM glipizid was found to have lethal effect on hepatocytes. 250 µM glipizide application has an antiproliferative effect on hepatocytes. IC50 values were determined as 72 µM after 24h glipizide administration. The AML12 hepatocytes were treated with 2.5, 5, 7.5, 10, 15, 25 ve 50 mg/ml acarbose. 25 ve 50 mg/ml acarbose applied cytotoxic effects on cells. IC50 values were determined as 23 mg/ml after 24h acarbose administration. 5, 10, 25, 50, 100, 150 and 250 mM metformin were applied to 3T3-L1 adipocyte cells. Administration of 25, 50 and 100 mM metformin showed a severe cytotoxic effect on hepatocyte cells. Application of 150 and 250 mM metformin showed lethal effect on hepatocytes. IC50 value at 24 hours was calculated as 2.3 mM as a result of metformin application.

3.3.Effects of Antidiabetic Drugs over Proliferation of AML12 Hepatocyte and 3T3-L1 co-culture

To investigate the effect of oral antidiabetic drugs on proliferation, co-culture cells were cultured for 24 h in standard medium (untreated). 100 µM, 250 µM and 500 µM glipizide were applied to the cell culture medium. 500 µM glipizid was found to have lethal effect on cells. 250 uM glipizide application has an antiproliferative effect on cells. IC50 values were determined as 41.5 µM after 24h glipizide administration. Co-culture cells were treated with 1, 2, 4, 5, 7.5 and 10 mg / ml acarbose. Doses of 4, 5, 7.5 and 10 mg / ml acarbose were found to have an inhibiting effect on the cells. IC50 values were determined as 5 mg/ml after 24h acarbose administration. 10, 25, 50, 75 and 100 mM metformin were applied to the cell culture medium. The doses of metformin were not found to have a lethal effect on the cells but were found to have a anti proliferative effect on the cells.

3.4.FTO, CD68, NIBAN and RAN Gene Expression Levels in Response to Oral Antidyabetic Drugs in 3T3-L1 Adipocytes

24h 180 µM concentration of glipizide administered increasing effect over NIBAN and RAN gene expressions respectively as 3.05, 2.296 (p=0.005) fold compared to control adipocytes. FTO and CD68 gene expression levels were found to decrease respectively as 0.631, 0.627 (p=0.005) (Table 1.). 24h 175mM concentration of metformin administered decreasing effect over FTO, CD68, NIBAN and RAN gene expressions respectively as 0.095, 0.652, 0.874, 0.783 (p=0.005) fold compared to control adipocytes **(Table 1.).**

Table 1. The effect of oral antidiabetic drugs on FTO, CD68, NIBAN and RAN gene expression levels in 3T3-L1 adipocytes

	FTO Gene Expression Mean±SE; median (min-max)	p	CD68 Gene Expression Mean±SE; median (min-max)	p	NIBAN Gene Expression Mean±SE; median (min-max)	p	RAN Gene Expression Mean±SE; median (min-max)	p
Control	1.0 ± 0.0		1.0 ± 0.0		1.0 ± 0.0		1.0 ± 0.0	
A4	0.09 ± 0.00; 0.09 (0.09-0.10)	0.005	0.65 ± 0.00; 0.65 (0.65-0.66)	0.005	0.87 ± 0.00; 087 (0.87-0.88)	0.005	0.78 ± 0.00; 0.78 (0.78-0.79)	0.005*
A5	0.35 ± 0.00; 0.35 (0.34-0.35)	0.005	2.19 ± 0.00; 2.19 (2.18-2.19)	0.005	3.15 ± 0.00; 3.15 (3.15-3.16)	0.005	0.95 ± 0.00; 0.95 (0.95-0.96)	0.005*

Values are given as mean ± standart error; median (minimum-maximum). n:5 **A3:** Adipocyte cells treated with 180µM glipizide for 24 hours. A4: Adipocyte cells treated with 175mM metformin for 24 hours. Adjusted significanse limir p:0.010*. (Performed with Mann-Whitney Tes. Each group was compared with control)

3.5.FTO, CD68 and RAN Gene Expression Levels in Response to Oral Antidyabetic Drugs in AML12 Hepatocytes

24h 72 µM concentration of glipizide administered increasing effect over FTO and RAN gene expressions were found to repectively as 2.059, 1.171 and CD68 gene expression level was found to decreasing effect 0.232 (p=0.005) fold compared to control hepatocytes **(Table 2.).** 24h 2.3 mM concentration of metformin administered decreasing effect over FTO, CD68 and RAN gene expressions respectively as 0.13, 0.359, 0.743 (p=0.005) fold compared to control hepatocytes **(Table 2.).** 24h 23 mg/ml concentration of acarbose administered increasing effect over RAN gene expression levels 3.132 fold compared to control hepatocytes. 24h 23mg/ml concentration of acarbose administered decreasing effect over FTO and CD68 gene expressions levels respectively as 0.089, 0.116 (p=0.005) fold compared to control hepatocytes **(Table 2.).**

Table 2. FTO, CD68 and RAN Gene Expression Levels in Response to Oral Antidyabetic Drugs in AML12 Hepatocytes

	FTO Gene Expression Mean±SE; median (min-max)	p	CD68 Gene Expression Mean±SE; median (min-max)	p	RAN Gene Expression Mean±SE; median (min-max)	p
Control	1.0 ± 0.0		1.0 ± 0.0		1.0 ± 0.0	
H1	2.06 ± 0.00; 2.06 (2.05-2.06)	0.005*	0.23 ± 0.00; 0.23 (0.23-0.24)	0.005*	1.17 ± 0.00; 1.17 (1.17-1.18)	0.005*
H2	0.13 ± 0.00; 0.13 (0.13-0.14)	0.005*	0.36 ± 0.00; 0.36 (0.35-0.36)	0.005*	0.74 ± 0.00; 0.74 (0.74-0.75)	0.005*
H3	0.09 ± 0.00; 0.09 (0.08-0.09)	0.005*	0.12 ± 0.00; 012 (0.11-0.12)	0.005*	3.13 ± 0.00; 3.13 (3.13-3.14)	0.005*

Values are given as mean ± standart error; median (minimum-maximum). n:5 **H1:** Hepatocyte cells treated with 72 µM glipizide for 24 hours. **H2:** Hepatocyte cells treated with 2.3mM metformin for 24 hours. **H3:** Hepatocyte cells treated with 23 mg/ml acarbose for 24 hours. Adjusted significanse limir p:0.010*. (Performed with Mann-Whitney Tes. Each group was compared with control)

3.6.FTO, CD68 and RAN gene expression levels in response to oral antidiabetic drugs in AML12 hepatocytes in co-culture

24h 41.5 µM concentration of glipizide administered increasing effect over FTO and CD68 gene expressions respectively as 1.229, 1.716 (p=0.005) fold compared to control hepatocytes in co-culture and RAN gene expression levels decreasing effect 0.000 fold compare to control cells (p = 0.005) **(Table 3.).**

24h 5mg/ml concentration of acarbose administered increasing effect over RAN gene expression levels 2.385 fold compared to control hepatocytes in co-culture. 24h 5mg/ml concentration of acarbose administered decreasing effect over FTO and CD68 gene expressions levels respectively as 0.796, 0.327 (p=0.005) fold compared to control hepatocytes in co-culture **(Table 3.).**

Table 3. FTO, CD68 and RAN gene expression levels in response to oral antidiabetic drugs in AML12 hepatocytes in co-culture

	FTO Gene Expression Mean±SE; median (min-max)	p	CD68 Gene Expression Mean±SE; median (min-max)	p	RAN Gene Expression Mean±SE; median (min-max)	p
Control	1.0 ± 0.0		1.0 ± 0.0		1.0 ± 0.0	
C1	1.23 ± 0.00; 1.23 (1.22-1.23)	0.005	1.72 ± 0.00; 1.72 (1.71-1.72)	0.005	0.00 ± 0.00; 0.00 (0.00-0.00)	-
C2	0.80 ± 0.00; 0.80 (0.79-0.80)	0.005	0.33 ± 0.00; 0.33 (0.32-0.33)	0.005	2.38 ± 0.00; 2.38 (2.38-2.39)	0.005

Values are given as mean ± standart error; median (minimum-maximum). n:5 C**1:** Hepatocyte cells treated with 41.5 µM glipizide for 24 hours. **C2:** Hepatocyte cells treated with 5 mg/ml acarbose for 24 hours. Adjusted significanse limir p:0.010*. (Performed with Mann-Whitney Tes. Each group was compared with control)

3.7.FTO, CD68 and RAN gene expression levels in response to oral antidiabetic drugs in 3T3-L1 adipocytes in co-culture

We demonstrated that 24h, 41.5 µM glipizide have increasing effect over RAN gene expression as 5.287 fold to that of control cells adipocytes in co-culture whereas 41.5 µM glipizide have decreasing effect over FTO, CD68 and NIBAN gene expressions respectively as after 0.122, 0.338, 0.525 24h administration **(Table 4.).**

We demonstrated that 24h, 5mg/ml acarbose have increasing effect over NIBAN and RAN gene expression respectively as 3.11, 1.58 fold to that of control cells adipocytes in co-culture whereas 5mg/ml acarbose have decreasing effect over FTO and CD68 gene expressions respectively as after 0.027, 0.165 24h administration **(Table 4.).**

Table 4. FTO, CD68 and RAN gene expression levels in response to oral antidiabetic drugs in 3T3-L1 adipocytes in co-culture

	FTO Gene Expression Mean±SE; median (min-max)	p	CD68 Gene Expression Mean±SE; median (min-max)	p	NIBAN Gene Expression Mean±SE; median (min-max)	p	RAN Gene Expression Mean±SE; median (min-max)	p
Control	1.0 ± 0.0		1.0 ± 0.0		1.0 ± 0.0		1.0 ± 0.0	
C3	0.12 ± 0.00; 0.12 (0.12-0.13)	0.005	0.34 ± 0.00; 0.34 (0.33-0.34)	0.005	0.52 ± 0.00; 0.52 (0.52 -0.53)	0.005	5.29 ± 0.00; 5.29 (5.28-5.29)	0.005
C4	0.03 ± 0.00; 0.03 (0.02-0.03)	0.005	0.16 ± 0.00; 0.16 (0.16-0.17)	0.005	3.11 ± 0.00; 3.11 (3.11-3.12)	0.005	1.58 ± 0.00; 1.58 (1.58-1.59)	0.005

Values are given as mean ± standart error; median (minimum-maximum). n:5 **C3:** Adipocyte cells treated with 41.5 µM glipizide for 24 hours. **C4:** Adipocyte cells treated with 5 mg/ml acarbose for 24 hours. Adjusted significanse limir p:0.010*. (Performed with Mann-Whitney Tes. Each group was compared with control)

4. Discussion

Obesity is strongly associated with the development of insulin resistance and is thought to be responsible for the development of type 2 diabetes. Although the epidemiological relationship has been established, the cellular linkage and molecular mechanisms between obesity and insulin resistance are still unknown. Increased obesity is associated with lipid accumulation in the liver. Although the role of visceral fat in the development of systemic insulin resistance is controversial, the contribution of visceral fat is important in the development of hepatic insulin resistance (Cai et al., 2005; Kim et al., 2003). it is predicted that visceral fat depot may induce liver insulin resistance and this station stimulates systemic insulin resistance (Wang et al., 2006). Several studies have shown that hepatic insulin resistance is associated with low-grade cellular inflammation (Cai et al., 2005; Arkan et al., 2005). Paracrine interaction between fat and liver can directly elicit an inflammatory response in liver cells, but this is not clearly known.

We demonstrated that AML12 hepatocytes, 3T3-L1 adipocytes and their co-culture FTO, CD68, NIBAN and RAN gene expressions in response to metformin, glipizide and acarbose exposure.

Animal model studies showed that FTO was positively associated with fat accumulation (McCarthy et al., 2010). In our study, we found that FTO gene expression level decreased 0.631 fold in 3T3-L1 adipocyte cells treated with 180 µM glipizide for 24 hours. Glipizide exposure may have a protective effect against insulin resistance in adipose tissue. In our study, it was found that the expression level of CD68 gene decreased by 0.627 times when the cells treated with 180 µM 24 hours glipizide were compared with the control cells. This may cure the insulin resistance in adipocyte cells and indicate that the inflammation there decreases. The mechanism by which the NIBAN gene, which is known to be involved in the adiponic process, is involved in this process remains unclear (Ye et al., 2011). It has been found that the NIBAN gene regulates cell death signals in response to endoplasmic reticulum stress and plays an anti-apoptotic role (Sun et al., 2007). In our study to determine the relationship between NIBAN gene and glipizide use, 3T3-L1 adipocytes treated with 180 µM glipizide for 24 hours compared to control cells were found to increase the NIBAN gene 3 fold. This may reflect the role of glipizide in the treatment of both obesity and diabetes in obese patients with T2DM by secreting insulin by trying to produce an anti-apoptotic effect. Ran protein is involved in the control of DNA synthesis and the functioning of the mitotic cell cycle, and during mitosis, regulation of molecules in microtubule polymerization may be key to signaling (Sazer et al., 2000). According to our study, when compared to control cells with adipocytes treated 24 hours 180 µM glipizide, RAN gene expression level was increased by 2,296 times. High RAN gene expression may have a regulatory effect on glucose homeostasis.

FTO, CD68, NIBAN and RAN gene expression were decreased in all groups in metformin treated cells. FTO inhibits gluconeogenesis and adipogenesis by balancing metformin activity (Melnik, 2015). Overexpression of the FTO gene causes an increase in gluconeogenesis and adipogenesis (Melnik, 2015). Increased FTO mRNA levels in subcutaneous adipose tissue in T2DM patients and treatment with rosiglitazone decreases FTO mRNA levels in subcutaneous adipose tissue by increasing insulin sensitivity (Bravard et al., 2013). The results of our study were reported by Bravard et al. (2013) is similar to his work. FTO gene expression level was decreased by 0.095 times when compared to control cells with 24 hours 175 mM metformin treated cells. Treatment of 3T3-L1 adipocyte cells with metformin increased insulin sensitivity in the cells, resulting in decreased FTO gene expression in adipocytes. CD68 is expressed in the stromal vascular fraction in human adipose tissues (Di Gregorio et al., 2005). Studies have shown that there is a significant infiltration of fat tissue by macrophages in obesity (Weisberg et al., 2003; Xu et al., 2003). Gregorio et al. in order to better understand the relationship between macrophage infiltration and insulin resistance in adipose tissue, they measured CD68 gene expression levels by giving patients metformin and pioglitazone (Di Gregorio et al., 2005). Found a relationship between impaired glucose

tolerance and decreased expression of CD68 (Di Gregorio et al., 2005). Zulian et al. (2011) found that metformin treatment in adipose tissue decreased CD68 gene expression statistically. We found that CD68 gene expression level decreased by 0.652 fold compared to control cells treated with 175 mM metformin for 24 hours. As a result of our study similar to the literature, we found that metformin reduced CD68 gene expression level and metformin plays a role in reducing regional inflammation in adipose tissue in vitro. Reduction of FTO and CD68 gene expression in metformin treated cells may indicate that it may have a protective effect on obesity and inflammation. 3T3-L1 cells treated with 175 mM metformin for 24 hours compared to control cells, NIBAN ge decreased 0.874 fold. Reduction of NIBAN gene expression by metformin administration may indicate mature adipocytes treatment. Our study is one of the first studies conducted in the literature to explain the relationship between obesity and RAN gene in adipogenic process. Adipocytes treated with 175 mM metformin for 24 hours compared to control cells, RAN gene expression level decreased 0.783 fold. The results of our study may reflect that metformin is a regulatory mechanism against impaired glucose homeostasis by reducing RAN gene expression in adipocytes.

Glipizide is metabolized mainly by the liver. Sulfonylureas may cause chronic hepatitis with necroinflammatory changes (Bloodworth et al., 1961). In our study, we applied 72 μM glipizide to AML12 hepatocytes for 24 hours and found that FTO gene expression level increased 2.059 times when hepatocyte cells and control cells were compared. In our study, we applied 72 μM glipizide to AML12 hepatocytes for 24 hours and we found that CD68 gene expression levels decreased 0.232 times when hepatocyte and control cells were compared. The decrease in the level of CD68 gene expression in the hepatocytes administered in glipizide suggests that it plays a role in reducing inflammation in the liver by reducing insulin resistance in hepatocytes. We exposed AML12 hepatocytes to 72μM glipizide for 24 hours, and it was found that RAN gene expression level increased 1.171 ($p = 0.005$) fold when hepatocyte cells and control cells were compared. Increased RAN expression with the dose administered may be due to the need for regulation of glucose homeostasis in the liver.

Metformin is not involved in hepatic metabolism and is excreted unchanged in the urine. Biguanides, such as metformin hydrochloride, have not been reported associated with liver damage (Sulkin et al., 1997). In our study, AML12 hepatocytes cells treated with 24 hours 2.3 mM metformin and compared to control cells, FTO gene expression level decreased 0.13 fold. This may indicate that metformin administration to hepatocytes decreases the amount of fat in the liver and that metformin has a protective effect on the liver. Treatment of hepatocytes with 2.3 mM metformin for 24 hours revealed that CD68 gene expression level decreased by 0.359 times. As a result of the application of metformin to the heptocyte cells decreased CD68 gene expression level showed that the inflammation in that region decreased and metformin in the treatment benefit. It was determined that the expression level of RAN gene decreased by 0.743 times when hepatocytes treated with 24 hours 2.3 mM metformin were compared with control cells. According to the study of transgenic mice, RAN signaling is essential for pancreatic islet development and glucose homeostasis (Xia et al., 2011). The dose of metformin administered may reflect the activity of regulating decreased glucose homeostasis in hepatocytes.

Alpha-glycosidase inhibitors may be particularly useful in patients with liver disease (Tolman et al., 2007). Rudovich et al. (2010) found that in combination with ezetimibe and acarbose to treat non-alcoholic fatty liver disease, liver fat, inflammation and fibrosis were significantly reduced. In our study, compared to AML12 hepatocyte cells treated with 23 mM acarbose for 24 hours and control cells, FTO gene expression level was decreased 0.089 times in substance treated cells. Reduction of FTO gene expression may indicate that administration of acarbose in a customized dose helps to reduce the amount of fat in hepatocytes. Treatment of hepatocytes with 23 mM acarbose for 24 hours revealed that CD68 gene expression level decreased 0.116 times. Reduction of CD68 gene expression as a result of acarbose administration shows that inflammation is reduced in the liver. Hepatocyte cells treated with 23 mM metformin for 24 hours compared to control cells were found to increase RAN gene expression level approximately 3 fold. This suggests that acarbose increases RAN gene expression to enable glucose hemeostasis.

In our study, we found that FTO gene expression level increased 1.229 times when 3T3-L1 adipocyte and AML12 hepatocyte co-culture hepatocytes were compared with control co-culture hepatocytes treated with 41.5 μM glipizide for 24 hours. Increased FTO gene expression in co-culture hepatocytes in which liver adiposity is modeled may indicate that adipocytes interact with hepatocyte cells to increase lipid levels, and may indicate that glipizide alone is not effective for treating fat in hepatocytes. Huang et al. (2010) found that CD68 macrophage infiltration increased in liver fat. ko-kültür hepatositlerinde CD68 gen anlatım seviyesinin 1.716 kat arttığı tespit edildi. This indicates that CD68 gene expression expression is increased in order to prevent inflammation in glipizide-treated hepatocytes in the co-culture.

In our study, we found that FTO gene expression level decreased by 0.796 times when 3T3-L1 adipocyte and AML12 hepatocyte co-culture hepatocytes were compared with control co-culture hepatocytes treated with 5 mg / ml acarbose for 24 hours. Reduction of FTO gene expression in hepatocyte cells in co-culture may indicate that lipid amounts in hepatocytes are reduced. When we compared the co-culture hepatocyte control cells by exposing hepatocytes to 5 mg / ml acarbose for 24 hours in 3T3-L1 adipocyte and AML12 hepatocyte co-culture, CD68 gene

expression level was found to be 0.327 fold decreased. This shows that inflammation in co-cultured hepatocyte cells is reduced. Acarbose is an alternative therapeutic to treat fats in hepatocytes. Treatment of co-culture hepatocyte cells with 5 mg / ml acarbose for 24 hours showed that RAN gene expression of acarbose increased by 2,385 fold. This shows that acarbose alone cannot maintain glucose balance and regulates glucose metabolism through RAN gene expression.

Adipocyte-mediated factors play a role in the development of hepatic insulin resistance (Zhou et al., 2007). Hepatic insulin resistance is responsible for the development of type 2 diabetes (Taniguchi et al., 2005). In our study, we found that FTO gene expression level decreased by 0.122 times when 3T3-L1 adipocyte and AML12 hepatocyte co-culture adipocytes were compared with control co-culture adipocytes treated with 41.5 μM glipizide for 24 hours. Reduction of FTO mRNA levels indicates that applied glipizide reduces adipocyte fat. When the adipocytes in the co-culture were exposed to 41.5 μM glipizide for 24 hours, it was found that CD68 gene expression level increased by 0.338 times when compared with the control co-culture adipocyte cells. Wang et al. (2006) showed that mature 3T3-L1 adipocytes are capable of stimulating NF-kB activation in hepatocytes. In our study, we determined that glipizide applied to adipocytes in the co-culture decreased the level of CD68 gene expression, indicating that it increases glucose usage in adipocytes and prevents inflammation by decreasing insulin resistance. Treatment of co-culture adipocyte cells with 41.5 μM glipizide for 24 hours showed that acarbose reduced NIBAN gene expression by 0.525 fold. Reduction of NIBAN gene expression by administration of glipizide may indicate that mature adipocytes are treated in co-culture.

In our study, we found that the FTO gene expression level decreased by 0.027 times when 3T3-L1 adipocyte and AML12 hepatocyte co-culture adipocytes were compared with control co-culture adipocytes treated with 24 hours 5 mg / ml acarbose. Reduction of FTO mRNA level indicates that acarbose reduces fat in adipocytes and and it indicates that trying to treat the adipocyte-induced fatty liver. When 3T3-L1 adipocyte and AML12 hepatocyte co-culture adipocytes were exposed to 5 mg / ml acarbose for 24 hours, CD68 gene expression level was reduced 0.165 fold. Decrease in CD68 gene expression level in acarbose-induced adipocytes in co-culture indicates that inflammation in adipocytes is reduced. Treatment of co-culture adipocytes with acarbose 5 mg / ml for 24 hours showed that acarbose increased NIBAN gene expression approximately 3 fold. Increased NIBAN gene expression by acarbose administration may reflect the anti-apoptotic effect of mature adipocytes in co-culture, which may help in the treatment of liver fats. Treatment of co-culture adipocytes with 5 mg / ml acarbose for 24 hours showed that acarbose increased RAN gene expression 1.58 fold. This suggests that acarbose increases RAN gene expression to enable glucose hemeostasis. Acarbose may be an alternative drug for the treatment of cells in the fatty liver model.

5. Conclusions

In conclusion, the reducing effect of oral antidiabetic drug on CD68 and FTO may prevent inflammation in hepatocyte and adipocyte cells. Antidiabetic drug apply to adipocytes and hepatocytes RAN gene may reflect the reduced glucose homeostasis regulatory activities of fatty liver models.

Acknowledgements
This work was supported by the Marmara University Scientific Research Projects Commission (Project No: FEN-C-DRP-131113-0433).

Authors' contributions:
Meliha Koldemir Gündüz: Project development and writing, application of experiments, result analysis, article writing
Mehtap Çevik: Application of experiments, article writing
Penbe Çağatay: Result analysis, article writing
Belgin Süsleyici: Project development and writing, application of experiments, result analysis, article writing

Conflict of interest disclosure:
There is no conflict of interest

References

Adachi H, Majima S, Kon S, Kobayashi T, Kajino K, Mitani H, Hirayama Y, Shiina H, Igawa M., Hino O 2004. Niban gene is commonly expressed in the renal tumors: a new candidate marker for renal carcinogenesis. Oncogene, 23(19), 3495-3500.

American Diabetes Association 2018. 2. Classification and diagnosis of diabetes: Standards of medical care in diabetes-2018. Diabetes Care, 41, 13-27.

Arkan MC, Hevener AL, Greten FR, Maeda S, Li ZW, Long JM 2005. IKK-b links inflammation to obesity-induced insulin resistance. Nat Med 11: 191–197.

Beyler AR, Aytaç Ş 2002. Nonalkolik Steatohepatitis. Gastroenteroloji, 593-600.

Bloodworth JMB, Hamwi GJ 1961. Histopathologic lesion associated with sulfonylurea administration. Diabetes, 10: 90-99.

Bravard A, Veilleux A, Disse E, Laville M, Vidal H, Tchernof A, Rieusset J 2013. The expression of FTO in human adipose tissue is influenced by fat depot, adiposity, and insulin sensitivity. Obesity (Silver Spring), 21, 1165–1173.

Cai DS, Yuan MS, Frantz DF, Melendez PA, Hansen L, Lee J 2005. Local and systemic insulin resistance resulting from hepatic activation of IKK-b and NF-jB. Nat Med, 11: 183–190.

Cancello R1, Henegar C, Viguerie N, Taleb S, Poitou C, Rouault C, Coupaye M, Pelloux V, Hugol D, Bouillot JL, Bouloumié A, Barbatelli G, Cinti S, Svensson PA, Barsh GS, Zucker JD, Basdevant A, Langin D, Clément K 2005. Reduction of macrophage infiltration and chemoattractant gene expression changes in white adipose tissue of morbidly obese subjects after surgery-induced weight loss. Diabetes, 54, 2277-2286.

Clarke, PR. Zhang, C 2008. Spatial and temporal coordination of mitosis by Ran GTPase. Nat Rev Mol Cell Biol, 9, 464–477.

Clément K, Viguerie N, Poitou C, Carette C, Pelloux V, Curat CA, Sicard A, Rome S, Benis A, Zucker JD, Vidal H, Laville M, Barsh GS, Basdevant A, Stich V, Cancello R, Langin D 2004. Weight loss regulates inflammation-related genes in white adipose tissue of obese subjects. The FASEB Journal 18, 1657-1669.

Demir, K 2004. Nonalkolik Yağlı Karaciğer Hastalığı:Etyoloji ve patogenez. Çapa Gastroenteroloji Günleri, 90-94.

Di Gregorio GB, Yao-Borengasser A, Rasouli N, Varma V, Lu T, Miles LM, Ranganathan G, Peterson CA, McGehee RE, Kern PA 2005. Expression of CD68 and macrophage chemoattractant protein-1 genes in human adipose and muscle tissues: association with cytokine expression, insulin resistance, and reduction by pioglitazone. Diabetes, 54(8): 2305-2313.

Dina C, Meyre D, Gallina S, Durand E, Körner A, Jacobson P, Carlsson LM, Kiess W, Vatin V, Lecoeur C, Delplanque J, Vaillant E, Pattou F, Ruiz J, Weill J, Levy-Marchal C, Horber F, Potoczna N, Hercberg S, Le Stunff C, Bougnères P, Kovacs P, Marre M, Balkau B, Cauchi S, Chèvre JC, Froguel P 2007. Variation in FTO contributes to childhood obesity and severe adult obesity. Nature Genetic 39, 724-726.

Frayling TM, Timpson NJ, Weedon MN, Zeggini E, Freathy RM, Lindgren CM, Perry JR, Elliott KS, Lango H, Rayner NW, Shields B, Harries LW, Barrett JC, Ellard S, Groves CJ, Knight B, Patch AM, Ness AR, Ebrahim S, Lawlor DA, Ring SM, Ben-Shlomo Y, Jarvelin MR, Sovio U, Bennett AJ, Melzer D, Ferrucci L, Loos RJ, Barroso I, Wareham NJ, Karpe F, Owen KR, Cardon LR, Walker M, Hitman GA, Palmer CN, Doney AS, Morris AD, Smith GD, Hattersley AT, McCarthy MI 2007. A common variant in the FTO gene is associated with body mass index and predisposes to childhood and adult obesity. Science 316, 889-894.

Huang W, Metlakunta A, Dedousis N, Zhang P, Sipula I, Dube JJ, Scott DK, O'Doherty RM 2010. Depletion of liver Kupffer cells prevents the development of diet-induced hepatic steatosis and insulin resistance. Diabetes, 59(2): 347-57.

Kim SP, Ellmerer M, Van Citters GW, Bergman RN 2003. Primary of hepatic insulin resistance in the development of the metabolic syndrome induced by an isocaloric moderate-fat diet in the dog. Diabetes, 52: 2453–2460.

Koldemir M, Kahveci C, Bayer H, Cagatay P, Yildiz S, Bagriacik N, Susleyici-Duman B 2012. Relationship of RIC-3 gene rs1528133 polymorphism with varying degrees of body weight and eating behavior. Diabetes Metab Syndr. 6(2):90-95.

Melnik BC 2015. Milk: an epigenetic amplifier of FTO- mediated transcription? Implications for Western diseases. Melnik J Transl Med, 13: 385.

Miard S, Dombrowski L, Carte, S, Boivin L, Picard F 2008. Aging alters PPARgamma in rodent and human adipose tissue by modulating the balance in steroid receptor coactivator-1. Aging Cell, 8(4):449-459.

McCarthy MI 2010. Genomics, type 2 diabetes, and obesity. N Engl J Med, 363(24), 2339-2350.

Niu L, Geyer PE, Wewer Albrechtsen NJ, Gluud LL, Santos A, Doll S, Treit PV, Holst JJ, Knop FK, Vilsbøll T, Junker A, Sachs S, Stemmer K, Müller TD, Tschöp MH, Hofmann SM, Mann M 2019. Plasma proteome profiling discovers novel proteins associated with non-alcoholic fatty liver disease. Mol Syst Biol. 1;15(3):e8793.

Prokopenko I, McCarthy MI, Lindgren CM 2008. Type 2 diabetes: new genes, new understanding. Trends in Genetics 24, 613-621.

Reaven GM 1995. Pathophysiology of insulin resistance in human disease. Physiol Rev 75, 473-486.

Rösen P, Nawroth PP, King G, Möller W, Tritschler HJ, Packer L 2001. The role of oxidative stress in the onset and progression of diabetes and its complications: a summary of a Congress Series sponsored by UNESCOMCBN, the American Diabetes Association and the German Diabetes Society. Diabetes/Metabolism Research and Reviews 17, 189–212.

Rudovich NN, Weickert MO, Andreas JM, Pfeiffer FH 2010. Combination of acarbose and ezetimibe prevents non-alcoholic fatty liver disease: A break of intestinal insulin resistance? Journal of Hepatology, 52(6): 952-953.

Samaras K, Botelho NK, Chisholm DJ, Lord RV 2010. Subcutaneous and Visceral Adipose Tissue FTO Gene Expression and Adiposity, Insulin Action, Glucose Metabolism, and Inflammatory Adipokines in Type 2 Diabetes Mellitus and in Health. Obesity Surgery 20, pp.108-113.

Sanyal AJ 2003. Nonalcoholic fatty liver and steatohepatitis: the hepatic manifestation of the insulin resistance syndrome. Presented at The First Annual World Congress on the Insulin Resistance Syndrome. November 20-22 Los Angeles, California.

Sazer S, Dasso M 2000. The ran decathlon: multiple roles of Ran. J Cell Sci, 113(7): 1111–1118.

Schlessinger D, Cao A, Lakatta E, Abecasis GR 2007. Genome-wide association scan shows genetic variants in the FTO gene are associated with obesity-related traits. PLoS Genetic 3, e115.

Scuteri A, Sanna S, Chen WM, Uda M, Albai G, Strait J, Najjar S, Nagaraja R, Orrú M, Usala G, Dei M, Lai S, Maschio A, Busonero F, Mulas A, Ehret GB, Fink AA, Weder AB, Cooper RS, Galan P, Chakravarti A, Segev N 2011. Coordination of intracellular transport steps by GTPases. Sem Cell Dev Biol, 22, 33–38.

Shoelson SE, Lee J, Goldfine AB 2006. Inflammation and insulin resistance. J Clin Invest, 116, 1793–1801.

Stratigopoulos G, Padilla SL, LeDuc CA, Watson E, Hattersley AT, McCarthy MI, Zeltser LM, Chung WK, Leibel RL 2008. Regulation of Fto/Ftm gene expression in mice and humans. American Journal of Physiology – Regulatory. Integrative and Comparative Physiology, 294, 1185–1196.

Sulkin TV, Bosman D, Krentz AJ 1997. Contraindications to metformin therapy in patients with NIDDM. Diabetes Care, 20: 925-928.

Sun GD, Kobayashi T, Abe M, Tada N, Adachi H, Shiota A, Totsuka Y, Hino O 2007. The endoplasmic reticulum stress-inducible protein Niban regulates eIF2α and S6K1/4E-BP1 phosphorylation. Biochem Biophys Res Commun, 360, 181–187.

Taniguchi CM, Ueki K, Kahn R 2005. Complementary roles of IRS-1 and IRS-2 in the hepatic regulation of metabolism. J Clin Invest, 115: 718–727.

Tolman KG, Fonseca V, Pharmd AD, Tan MH 2007. Spectrum of Liver Disease in Type 2 Diabetes and Management of Patients With Diabetes and Liver Disease. Diabetes Care, 30 (3).

Tükün A 2008. Diyabette Genetik Yükler. Türk Biyokimya Dergisi 33.

Vasanth Rao VRB, Candasamy M, Bhattamisra SK 2019. Obesity an overview: Genetic conditions and recent developments in therapeutic interventions. Diabetes & Metabolic Syndrome: Clinical Research & Reviews, 13, 2112-2120.

Wang Z, Lv J, Zhang R, Zhu Y, Zhu D, Sun Y, Zhu, J, Han X 2006. Co-culture with fat cells induces cellular insulin resistance in primary hepatocytes. Biochem Biophys Res Commun, 345(3): 976-83.

Weisberg SP, McCann D, Desai M, Rosenbaum M, Leibel RL, Ferrante AW Jr 2003. Obesity is associated with macrophage accumulation in adipose tissue. Journal of Clinical Investigation, 112, 1796-1808.

Wellen KE and Hotamisligil GS 2005. Inflammation, stress, and diabetes. J Clin Invest, 115, 1111–1119.

Xia F, Dohi T, Martin NM, Raskett CM, Liu Q, Altieri DC 2011. Essential Role of the Small GTPase Ran in Postnatal Pancreatic Islet Development. PLoS ONE 6(11), pp. e27879.

Xu H, Barnes GT, Yang Q, Tan G, Yang D, Chou CJ, Sole J, Nichols A, Ross JS, Tartaglia LA, Chen H 2003. Chronic inflammation in fat plays a crucial role in the development of obesity-related insulin resistance. J Clin Invest, 112: 1821–1830.

Yaribeygi H, Simental-Mendía LE, Barreto GE, Sahebkar A 2019. Metabolic effects of antidiabetic drugs on adipocytes and adipokine expression. J Cell Physiol, 1-11.

Ye F, Zhang H, Yang YX, Hu HD, Sze SK, Meng W, Qian J, Ren H, Yang BL, Luo MY, Wu X, Zhu W, Cai WJ, Tong JB 2011. Comparative Proteome Analysis of 3T3-L1 Adipocyte Differentiation Using iTRAQ-Coupled 2D LC-MS/MS. Journal of Cellular Biochemistry, 112, 3002– 3017

Younossi ZM, Blissett D, Blissett R, Henry L, Stepanova M, Younossi Y, Racila A, Hunt S, Beckerman R 2016. The economic and clinical burden of nonalcoholic fatty liver disease in the United States and Europe. Hepatology, 64: 1577 – 1586.

Yuzbashian E, Asghari G, Hedayati M, Zarkesh M, Mirmiran P, Khalaj A 2019. The association of dietary carbohydrate with FTO gene expression in visceral and subcutaneous adipose tissue of adults without diabetes. Nutrition, 63-64:92-97.

Yudin D, Fainzilber M 2009. Ran on tracks-cytoplasmic roles for a nuclear regulator. J Cell Sci, 122, 587-593.

Zhou L, Sell H, Eckardt K, Yang Z, Eckel J 2007. Conditioned medium obtained from in vitro differentiated adipocytes and resistin induce insulin resistance in human hepatocytes. FEBS Lett, 581(22): 4303-4308.

Zulian A, Cancello R, Girola A, Gilardini L, Alberti L, Croci M, Micheletto G, Danelli P, Invitti C 2011. In vitro and in vivo effects of metformin on human adipose tissue adiponectin. Obes Facts, 4(1):27-33.

EJBCS